ASTROBIOLOGY
Volume 24, Number 12, 2024
Mary Ann Liebert, Inc.
DOI: 10.1089/ast.2024.0047

Open camera or QR reader and scan code to access this article and other resources online.

Organic Products of Fatty Acid and Magnesium Sulfate Mixtures after Gamma Radiolysis: Implications for Missions to Europa

James M.T. Lewis,[1–3] Dina M. Bower,[2,4] Alexander A. Pavlov,[2] Xiang Li,[2] Sarinah Z. Wahl,[2,3,5] Jennifer L. Eigenbrode,[2] and Amy C. McAdam[2]

Abstract

If ocean-derived materials are present at Europa's surface, they would represent accessible records of ocean chemistry and habitability, but such materials would be further processed by Europa's harsh radiation environment. In this study, saturated fatty acids were precipitated onto a Europa-relevant hydrated magnesium sulfate and exposed to gamma radiation doses up to 2 MGy at −196°C. Alkane chains, with carbon numbers one less than those of the starting fatty acids, were the most abundant radiolysis products in solvent and thermal extracts analyzed by gas chromatography mass spectrometry. Detections of monounsaturated fatty acids and combined radiolysis products were attributed to the experiment's Europa-like parameters. Additionally, elevated concentrations of shorter-chain saturated fatty acids suggest that gamma radiation induced charge remote fragmentation of the alkyl chains of some starting fatty acids under these experimental conditions. Quantitation of fatty acid concentrations in the irradiated samples enabled the calculation of a radiolysis constant that indicated exposure to a 5 MGy dose of gamma radiation would have resulted in a ∼90% loss of the initial fatty acid population. The samples were further studied by Raman spectroscopy and laser desorption and ionization mass spectrometry, which characterized the distribution of fatty acids and their radiolysis products on sulfate surfaces. The substantial loss of starting fatty acids typically seen with increasing radiation dose, along with the remarkable diversity of radiolysis products identified, suggests that the detection of fatty acids in irradiated sulfate deposits on Europa will be challenged by rapid destruction of any initial fatty acid populations and scrambling of their residual signals by a myriad of organic radiolysis products. If missions to Europa encounter sulfate deposits, targeting minimally irradiated units may still enable the detection of surviving fatty acid signatures that could inform about Europa's subsurface chemistry and habitability. Key Words: radiation—lipids—mass spectrometry—Raman spectroscopy—pyrolysis—kieserite. Astrobiology 24, 1166–1186.

1. Introduction

Characterizing the organic chemistry of planetary bodies is an essential component of determining their past and present habitability and distinguishing biotic from abiotic systems (Barge *et al*., 2022; Cockell *et al*., 2016; Eigenbrode, 2008; McKay 2020, Méndez *et al*., 2021; Parnell *et al*., 2007; Sephton and Botta, 2005; 2008; Summons *et al*., 2008). However, most solar system objects lack a thick atmosphere that would shield organic compounds from exogenous

[1]Department of Physics and Astronomy, Howard University, Washington, District of Columbia, USA.
[2]NASA Goddard Space Flight Center, Greenbelt, Maryland, USA.
[3]Center for Research and Exploration in Space Science and Technology, NASA GSFC, Greenbelt, Maryland, USA.
[4]Department of Astronomy, University of Maryland, College Park, Maryland, USA.
[5]Southeastern Universities Research Association, Washington, District of Columbia, USA.

sources of ionizing radiation, and they typically do not possess sedimentary environments that would favor the rapid burial and long-term preservation of organic signatures (Broz, 2020; Dartnell, 2011; Eigenbrode, 2008; Gerakines *et al*., 2022; Hedges and Keil, 1995; Kminek and Bada, 2006; Materese *et al*., 2020; Nordheim *et al*., 2018; 2022; Pavlov *et al*., 2012; 2022; 2024; Summons *et al*., 2008). For example, high-energy particles trapped within Jupiter's magnetosphere directly impact the surface of its moon Europa, and our limited understanding of the age range and dynamics of europan crustal materials makes it unclear whether any minimally irradiated near-surface organic records might persist (Johnson *et al*., 2004; Marion *et al*., 2003; Nordheim *et al*., 2018; 2022; Paranicas *et al*., 2007; 2009; Pavlov *et al*., 2024; Schmidt *et al*., 2011). There exist no natural terrestrial analogs to Europa's intensely irradiated surface, and thus laboratory investigations that subject organic-hosting samples to elevated doses of ionizing radiation are of critical importance. In this work, fatty acids were mixed with a hydrated sulfate salt suspected to be widespread on Europa, exposed to radiation doses and temperatures relevant to Europa's near-surface, and analyzed by a suite of analytical techniques. The results elucidate some of the organic radiolysis products that may be encountered in irradiated sulfate-rich terrains on Europa and the mechanisms of their formation.

Europa is a high-priority target for astrobiology missions as spacecraft and ground observations have identified compelling evidence for a long-lived liquid water ocean present below the moon's icy crust (Carr *et al*., 1998; Chyba and Phillips, 2002; Hand *et al*., 2009; Hand and Carlson, 2015; Kargel *et al*., 2000; Kivelson *et al*., 2000; Schmidt *et al*., 2011; Schubert *et al*., 2009; Sparks *et al*., 2017). Europa's low crater density and geomorphology suggest an active crust that may permit the exchange of materials between the ocean and surface (Greeley *et al*., 2000; 2004; Greenberg, 2010; Greenberg *et al*., 2000). While Europa's exterior is predominantly composed of water ice, it also exhibits spectral features indicative of the presence of salts (Brown and Hand, 2013; Carlson *et al*., 1999; Greeley *et al*., 2004; Hibbitts *et al*., 2019). Any salt deposits with structures and compositions suggestive of a deep subsurface origin would be primary targets for lander missions seeking to assess the chemistry of the europan ocean. An additional motivation for such efforts would be the opportunity to examine surface materials rich in radiolytic products (e.g., oxidants, radicals, and simple organic compounds). If crustal dynamics on Europa regularly transport radiolysis products down to the ocean, they could represent an important source of life-supporting ingredients (Chyba, 2000; Hand *et al*., 2009).

The magnetospheric charged particles that bombard and modify Europa's surface consist predominantly of energetic electrons but also include sulfur and oxygen ions sourced from volcanic eruptions on Io (Carlson *et al*., 1999; Johnson *et al*., 2004; Nordheim *et al*., 2018; 2022; Paranicas *et al*., 2002; 2007; 2009). The surface flux and spatial bombardment patterns of electrons and ions across Europa could be extremely variable due to the wide range of energies exhibited by impacting particles and the influences of Europa's ionosphere and the induced magnetic field of its subsurface ocean (Nordheim *et al*., 2022). Additionally, the jovian magnetosphere rotates faster than the orbital velocity of Europa, which results in electrons with energies <20 MeV flowing preferentially onto the hemisphere trailing Europa's motion and electrons with energies >20 MeV flowing preferentially onto the leading hemisphere (Nordheim *et al*., 2018; Paranicas *et al*., 2007; 2009). Spectra obtained by the near-infrared mapping spectrometer on board the Galileo spacecraft revealed the ubiquitous presence of hydrated sulfuric acid bearing terrains on Europa (Carlson *et al*., 1999). These terrains were found to be most abundant on the trailing hemisphere and were interpreted to have an origin potentially related to the impacts of magnetospheric sulfur ions (Carlson *et al*., 1999). Observations by Brown and Hand (2013) using the W. M. Keck Observatory identified an unknown infrared absorption feature that correlated with the spatial distribution of hydrated sulfuric acid on the trailing hemisphere, with the only plausible spectral matches found to be a magnesium sulfate brine or magnesium sulfate heptahydrate. Brown and Hand (2013) were unable to make any clear detections of sulfates on Europa's leading hemisphere and concluded that the magnesium sulfate was a probable radiation product formed by interactions between impacting sulfur ions and europan magnesium salts (e.g., magnesium chloride). However, modeling by Nordheim *et al*. (2022) found that sulfur ions may, in fact, have limited access to the trailing hemisphere and instead the bombardment of <20 MeV electrons could play a major role in the formation of hydrated sulfuric acid and hydrated magnesium sulfates found in this region. Dark materials found in linea, lenticulae, and chaos regions across Europa exhibit spectra consistent with hydrated sulfates (Carlson *et al*., 1999; Dalton *et al*., 2005), which potentially indicates that hydrated magnesium sulfates could be widespread.

In this present study, we examined how long-chained and very-long-chained alkyl carboxylic acids, herein referred to as fatty acids, decomposed when they were mixed with a hydrated magnesium sulfate powder and irradiated under Europa-like conditions. Fatty acids are of significant astrobiological interest in that (1) they are critical for the synthesis of compounds that form cellular membranes and energy stores in terrestrial organisms (Eigenbrode, 2008; Georgiou and Deamer, 2014; Summons *et al*., 2008), (2) they can form vesicles, due to their amphiphilic nature, that may have acted as protocells on prebiotic Earth (Jordan *et al*., 2019), and (3) fatty acids can act as long-lived molecular records of ancient life and environmental conditions (Eigenbrode, 2008; Summons *et al*., 2008). It is likely that abiotic fatty acids will have been regularly supplied to the Europa system via meteoritic infall (Cohen *et al*., 2023; Lai *et al*., 2019). It is also possible that fatty acids derived from ocean and crustal processes could be transported to the surface (Chivers *et al*., 2023; Chyba, 2000; Hand *et al*., 2009). Terrestrial organisms are known to produce fatty acid distributions that demonstrate a preference for particular chain lengths (Eigenbrode, 2008; Summons *et al*., 2008). Thus, if a similar patterning is observed in the chain length distributions of fatty acids detected on Europa, it would be interpreted to represent a possible biosignature (Eigenbrode, 2008; Georgiou and Deamer, 2014; Summons *et al*, 2008).

In the laboratory investigation reported here, synthetic sulfate-fatty-acid mixtures were exposed to $\sim$1 MeV gamma

rays, at doses of 0.2–2 MGy, and at temperatures (−196°C) similar to those of Europa's global mean annual surface temperature (−183°C) (Ashkenazy, 2019). Gamma rays were selected for this work, as at depths beyond a few centimeters to decimeters in Europa's subsurface, the radiation resulting from energetic electron impacts will consist predominantly of secondary bremsstrahlung radiation, including gamma-ray photons (Carlson *et al*., 1999; Johnson *et al*., 2004; Nordheim *et al*., 2018; Paranicas *et al*., 2002; 2007; 2009; Pavlov *et al*., 2024). The exact depth at which bremsstrahlung radiation becomes dominant will vary depending on the energy of the impacting electrons and the density of the target; in salt deposits this transition may overlap with expected sampling depths for a Europa lander ($\sim$0.5–2 cm and 5–10 cm) (Nordheim *et al*., 2018; Pappalardo *et al*., 2013). The findings of this investigation are also applicable to samples acquired at extremely shallow depths, as gamma rays interact with matter in a similar way to energetic electrons (Paranicas *et al*., 2001; Woo and Sandford, 2002). Additionally, the use of $\sim$1 MeV gamma rays had the practical advantage of not inducing radioactivity in the samples, thus facilitating their timely analysis with a large number of analytical techniques (Olszyna-Marzys, 1991). The gamma irradiated samples were analyzed quantitatively via gas chromatography mass spectrometry (GCMS) of solvent extracts and qualitatively with pyrolysis-GCMS, evolved gas analysis mass spectrometry (EGA-MS), Raman spectroscopy, and laser desorption and ionization mass spectrometry (LDI-MS). The data inform as to how effectively these different techniques can detect fatty acids associated with hydrated magnesium sulfate salts in non-irradiated and irradiated settings.

Previous studies have demonstrated that the gamma radiolysis of organic compounds follows preferred pathways influenced by molecular structures, and in the case of free C_n fatty acids, this typically involves α-cleavage in the vicinity of the carbonyl group to produce C_{n-1} hydrocarbons (Supplementary Fig. S1) (Dubravcic and Nawar, 1968; 1976; Kim *et al*., 2004; Nawar, 1978; Vajdi *et al*., 1978; Wu and Howton, 1975). Additional reported products include C_{n-2} alkenes and aldehydes of the same chain length as the parent fatty acid (Supplementary Fig. S1 and Supplementary Table S1) (Dubravcic and Nawar, 1976; Kim *et al*., 2004). For unsaturated free fatty acids, radiation-induced cleavage can also preferentially occur at double bond sites, which reduces the probability of a cleavage near the carbonyl group (Dubravcic and Nawar, 1968; Vajdi *et al*., 1978). While most fatty acid radiolysis studies are conducted with poorly ordered lipids in the liquid phase, Hau and Nawar (1986) investigated the irradiation of well-ordered monolayers of fatty acids adsorbed onto silica surfaces and observed changes in the relative proportions of radiolysis products. Here, we characterized the array of organic species produced by gamma radiolysis of saturated fatty acids precipitated onto the surface of a hydrated magnesium sulfate salt. The results inform as to some of the organic compounds that may be encountered in irradiated salt deposits on Europa.

2. Materials and Methods

2.1. Preparation of salt and fatty acid mixtures

Tetradecanoic acid (C14:0 FA), tetracosanoic acid (C24:0 FA), and magnesium sulfate monohydrate ($MgSO_4{\cdot}H_2O$) were sourced from Sigma-Aldrich. The $MgSO_4{\cdot}H_2O$ powder and C14:0 FA and C24:0 FA were mixed in dichloromethane (DCM, Fisher Scientific GC Resolve, amylene-stabilized) by using a Buchi rotary evaporator. Fatty acids are readily soluble in DCM, while $MgSO_4{\cdot}H_2O$ is not, so as the salt powder and solvent were agitated and dried by the rotary evaporator, a proportion of the fatty acids would have precipitated onto the solid salt. Due to the unknown rate of fatty acid radiolysis on $MgSO_4{\cdot}H_2O$, elevated amounts of C14:0 FA and C24:0 FA were utilized, so that if all the doped fatty acids were deposited on the 3 g of $MgSO_4{\cdot}H_2O$ present in the rotary evaporator flask, they would be mixed with the salt at a concentration of 2,700 ppm each by mass and their radiolysis products would likely be detectable with our analytical techniques (8 mg C14:0 FA added, 12 nmol C14:0 FA/mg salt; 8 mg C24:0 FA added, 7 nmol C24:0 FA/mg salt). Once the mixture had completely dried down, 300 mg aliquots of the homogenized powder were added to prescored Sigma-Aldrich long stem Vacule cryogenic ampules with a capacity of 1 mL. Any remaining powder was added to a solvent-cleaned 4 mL vial and stored as a reference mixture. The sample ampules were connected to a vacuum glass line and flame-sealed with a butane torch $\sim$3 cm above each ampule's prescored ring. The sealed ampules were stored at –20°C prior to irradiation.

2.2. Gamma irradiation of salt and fatty acid mixtures

The irradiation experiments were conducted at the Radiation Science & Engineering Center (RSEC) facility located at Pennsylvania State University, with the samples transported to and from the RSEC in an insulated container cooled with dry CO_2 ice. The ampules were placed in a circular metal holder and continuously cooled with liquid nitrogen while being exposed to $\sim$1 MeV gamma rays emitted from a ^{60}Co source until cumulative doses of 0.2, 0.5, 1, and 2 MGy were reached. A full description of the liquid nitrogen cooled radiation procedure employed here and the RSEC facilities are provided in the main text and supporting materials of Pavlov *et al*. (2024). Each ampule was stored in liquid nitrogen after its removal from the radiation chamber. Upon their return from the RSEC, the irradiated ampules were stored in a –80°C freezer prior to analysis.

Before the ampules were opened, they were allowed to equilibrate to room temperature, and the exteriors were rinsed in methanol, DCM-methanol (1:1 by volume), and DCM to remove contaminants that might transfer to the samples. The ampules were broken at their prescored rings, and the non-irradiated control and irradiated powders were transferred into ashed glass vials with solvent-cleaned caps using solvent-cleaned metal tools and then stored at –20°C.

2.3. Gas chromatography mass spectrometry of methylated solvent extracts

Methylated solvent extracts of the control and irradiated mixtures were generated to enable quantitative analysis of sample organics by GCMS. For each sample powder, three 10 mg aliquots were extracted, so that the uncertainty resulting from sample heterogeneity could be quantified. Each aliquot was placed in an ashed glass vial, immersed in 750 μL DCM, and vortexed for 10 s. The vial was centrifuged at 300

rpm for 1 min, and a solvent-cleaned glass syringe was used to transfer the supernatant into a separate vial. This process was repeated two more times, with all three supernatants collected into the same vial. As with the drying of all solvents in this study, the combined solvent extracts were dried under a gentle flow of purified N_2 gas.

Two approaches were utilized to hydrolyze and methylate sample compounds, including the doped fatty acids, into methyl esters (e.g., fatty acid methyl esters [FAMEs]) using trimethylsulfonium hydroxide (TMSH) solution ($\sim$0.25M in methanol) from Sigma-Aldrich. The standard approach used for the majority of analyses followed that of Müller *et al.* (1990) and Müller *et al.* (1998), in which 20 μL of TMSH solution was added to the dry extract at room temperature and vortexed for 15 s for immediate hydrolysis and methylation without heat augmentation. The methanol was dried, and the residue containing FAMEs, other derivatives, and any non-reactive radiolysis products (e.g., alkanes) was dissolved in 50 μL of a DCM stock solution that contained 50 μg/mL of *n*-heptadecane (n-C_{17} alkane) as an internal standard. The internal standard mitigated against uncertainty introduced when measuring 1 μL sample volumes with the 10-μL syringe used for manual injection of the extracts into the GCMS inlet. An optimized methylation method was implemented for a limited subset of samples to verify observations from the standard method. The optimized method used more TMSH (100 μl) and then applied heat (35°C for 30 min) after vortexing, which is consistent with thermally assisted hydrolysis and methylation (THM) methods of Shadkami *et al.* (2009) and Gries *et al.* (2021). This alternative method was explored as a path to potentially improve methylation reaction efficiencies.

The methylated extracts were analyzed with an Agilent 7890A gas chromatograph and Agilent 5975C mass spectrometer. The GC was equipped with a multimode inlet that enabled purging of the majority of the solvent and a focused introduction of analytes to the GC column. The inlet was operated under a helium pressure of 1 bar, held at 70°C for 1 min, ramped at a rate of 100°C/min to 320°C, and held for 3 min. Splitless injection was used to optimize the detection of low abundance radiolysis products. The GC oven was heated at a rate of 8°C/min from 70°C to 300°C where it was held for 10 min. The column flow was 0.9241 mL/min. The transfer line from the GC column to the MS was held at 280°C throughout the run. The MS source was held at 230°C and the MS quad at 150°C. The MS was operated with a solvent delay of 12 min, then continuously scanned 50–500 mass to charge ratio (*m/z*) range.

The GCMS data were analyzed by using Agilent's MSD Chemstation software with chromatogram peaks of interest identified through comparison with the NIST 08 spectral library. If a library entry was not available, the structure was deduced by *de novo* interpretation of the mass spectrum. If a total ion chromatogram peak was sufficiently above instrument background and did not co-elute with other species, the peak area was determined by using Chemstation's manual integration function. If these requirements were not met, an extracted ion chromatogram was generated, and the peak area was measured by Chemstation's integrate and label peak areas function.

Calibration curves were generated for C10:0–C24:0 FAMEs, C14:1 and C24:1 FAMEs, and *n*-tricosane (n-C_{23} alkane) relative to the n-C_{17} alkane used as an internal standard. This was achieved by combining the Sigma-Aldrich Supelco 37 component FAME mix with an n-C_{23} alkane stock solution, which was then mixed with an n-C_{17} alkane stock solution at a range of mixing ratios. Each mixture was analyzed in triplicate by GCMS. The average ratio of each analyte's chromatogram peak area to the n-C_{17} alkane peak area for each triplicate was plotted against the molar concentration ratio of the analyte to the n-C_{17} alkane.

For quantification of analytes in sample extracts, the ratio of each analyte peak area to the n-C_{17} alkane peak area in the same run was divided by the gradient of the relevant calibration curve plot to give the molar concentration ratio. This ratio was multiplied by the known molar concentration of the internal standard in the extract to find the molar concentration of the analyte, which was then multiplied by its molecular mass. For FAMEs, the molecular mass of the corresponding fatty acid was used to convert from the methyl ester to the parent fatty acid. The total amount of analyte in the 50 μL extract was determined by using the calculated molar concentration and divided by the mass of sample extracted to give the analyte concentration in μg per mg of sample. The analyte concentrations calculated for each triplicate set of sample aliquots were averaged and converted to average ppm and pmol/mg. The 1σ standard deviation of the average concentration was converted to relative uncertainty and combined with the relative uncertainties of the mass balance used for weighing the n-C_{17} alkane internal standard, the syringe used to measure the volume of solvent used for the internal standard solution, the molecular mass of each analyte, and the mass balance used to weigh out the solid sample aliquots. The total relative error was then converted to absolute error.

2.4. Raman spectroscopy

Raman measurements were performed on sample powders with a WITec α-Scanning Near-Field Optical Microscope customized to incorporate confocal visible wavelength (532 nm) Raman spectroscopy imaging utilizing 50x and 100x objectives to achieve a lateral resolution of $\sim$300 nm and a spot size of $\sim$1 μm. Spot scans and line scans of the sample surfaces were done using low laser power to avoid sample damage ($\sim$0.05–3 mW) with acquisition times $\sim$3–20 s/spot. To support data interpretation, Raman spectra were also collected from pure C14:0 FA, C24:0 FA, and n-C_{23} alkane powders. WITec Project Plus software was used to process the Raman data with Gaussian-Lorentzian fitting for baseline correction peak assignments. The WITec instrument is a low fidelity analog instrument for flight-like instrumentation but provides data analogous to what might be expected of Europa missions. Application of Raman spectroscopy to Europa Lander mission concepts is actively being developed (e.g., Sharma *et al.*, 2020; Vitkova *et al.*, 2022) and is part of NASA's Mars 2020 Perseverance rover and ESA's ExoMars Rosalind Franklin rover payloads as Scanning Habitable Environments with Raman and Luminescence for Organics and Chemicals (Sharma *et al.*, 2023) and the ExoMars Raman Laser Spectrometer (Veneranda *et al.*, 2020), respectively.

2.5. Laser desorption and ionization mass spectrometry

Each powdered sample was analyzed by a commercial matrix-assisted laser desorption/ionization time-of-flight mass spectrometer (Bruker Autoflex Speed). The powders were pressed onto a customized sample stub and introduced to the instrument. The ion source was equipped with a Nd:YAG laser (355 nm, <5 ns pulse) focused to an elliptical spot with approximate dimensions of 0.2 × 0.2 mm. The specific focus of this investigation was to detect the doped fatty acids in the negative ion mode, due to their tendency to lose a proton upon laser ablation, which results in the formation of deprotonated negative ions. The benchtop laser desorption and ionization mass spectrometry applied here is analogous to the instrumentation being deployed on the Rosalind Franklin rover in the Mars Organic Molecular Analyzer (Brinckerhoff *et al*., 2013) and on NASA's 2026 Dragonfly mission to Titan (Trainer *et al*., 2021).

2.6. Evolved gas analysis mass spectrometry

EGA-MS evaluates the thermal release of gases from bulk samples without additional preparations, which enables an assessment of how organic molecules are retained within mineral matrices (e.g., Boynton *et al*., 2001; Glavin *et al*., 2013 Eigenbrode *et al*. 2018; Holdiness, 1984; Mahaffy *et al*., 2012), much like Rock-Eval used by the petroleum industry (e.g., Scheeder *et al*., 2020), but supplemented with mass spectral information. EGA-MS was performed on 1 mg aliquots of the non-irradiated control and 0.5–2 MGy irradiated samples shortly after opening the ampules. Each sample powder was loaded into an ashed Frontier Laboratories stainless steel Eco-Cup and then heated in a Frontier Laboratories 3030D Multi-Shot Pyrolyzer. The pyrolyzer method was programed to ramp the oven from 50°C to 75°C in 75 s and then hold at 75°C for 528 s to release weakly adsorbed volatiles. The sample was heated to 850°C at a rate of 35°C/min, with a hold at 850°C for 360 s. The evolved gases were swept by 30 mbar He at a flow rate of 50 mL/min and a split of 100:1 to an Agilent LTM-5975T GCMS, with the GC column replaced by a filmless Frontier Laboratories deactivated Ultra Alloy UADTM-2.5N column (0.15 mm internal diameter, 2.5 m length), which enabled a direct connection between the inlet and the MS. The GC inlet, oven, and MSD transfer line were held at an isotherm of 135°C. These parameters were modeled after those used for EGA-MS experiments with the Sample Analysis at Mars instrument suite on board the Mars Science Laboratory Curiosity rover (Eigenbrode *et al*., 2018; Glavin *et al*., 2013; Lewis *et al*., 2021; Mahaffy *et al*., 2012).

2.7. Stepped pyrolysis gas chromatography mass spectrometry

Stepped pyrolysis GCMS was conducted by using an Agilent 7890A-5975C GCMS coupled to a Frontier Laboratories 3030D Multi-Shot Pyrolyzer to help deconvolve the EGA-MS results. Sample powders were loaded into a Frontier Laboratories stainless steel Eco-Cup and manually inserted into the pyrolyzer. The pyrolysis oven was held at 150°C for 2 min, ramped to 200°C at a rate of 600°C/min, held for 2 min, and then cooled to 150°C. The evolved gases were swept into the inlet of the GCMS by a He flow. The inlet was operated under a helium pressure of 0.4955 bar, with a total flow of 54 mL/min, and a split flow of 50:1. The inlet was held at 50°C for 15 min and then ramped at a rate of 100°C/min to 310°C and held for 10 min. The GC oven was held at 50°C (23 min) to focus analytes. The inlet was then allowed to cool to 80°C, while the oven was heated at a rate of 3°C/min to 250°C and held for 5 min, before ramping at a rate of 7°C per minute to 305°C, with a final hold of 2 min. The MS was operated with a solvent delay of 10 min and scanned the 50–450 *m/z* range. After completion of the GCMS run, the sample was kept in the pyrolyzer for the second heating step. The oven was held at 150°C for 2 min, ramped to 400°C at a rate of 600°C/min, held for 2 min, and cooled to 150°C. After the GCMS analysis of the evolved gases was completed, a third step with heating up to 600°C was used.

3. Results

3.1. Organic species produced by gamma radiolysis of fatty acids on hydrated magnesium sulfate

The irradiated samples were found to contain a diverse array of organic species formed by gamma radiolysis of the starting C14:0 FA and C24:0 FA (Fig. 1). The formulae of species detected or inferred by our methods and their systematic names are provided in Supplementary Table S1. Sections 3.1.1 and 3.1.2 focus on the abundant alkane and monounsaturated fatty acid products identified in extracts by GCMS. Section 3.1.3 details GCMS detections of compounds that were interpreted to have formed by radiolysis products combining. Section 3.2 describes how the population of detected saturated fatty acids in extracts changed with radiation dose, including the loss rate of starting fatty acids. Sections 3.3–3.6 outline the findings of investigations conducted by Raman spectroscopy, LDI-MS, EGA-MS, and pyrolysis-GCMS, respectively.

3.1.1. Alkanes. n-C_{23} alkane was detected in every irradiated sample, and its abundance increased with radiation dose (Table 1; Fig. 1, Column 2; Supplementary Table S2). It was inferred that n-C_{23} alkane was formed through the α-cleavage of C24:0 FA by gamma radiation to produce the C_{n-1} hydrocarbon, which is consistent with existing literature on the radiolysis of fatty acids (Supplementary Fig. S1) (Dubravcic and Nawar, 1968; 1976; Kim *et al*., 2004; Nawar, 1978; Vajdi *et al*., 1978; Wu and Howton, 1975). Of all the radiolysis products quantified in the samples, n-C_{23} alkane was by far the most abundant.

The detection of n-C_{23} alkane and reports from previously published work (Dubravcic and Nawar, 1968; 1976; Kim *et al*., 2004; Nawar, 1978; Vajdi *et al*., 1978; Wu and Howton, 1975) suggest that the doped C14:0 FA would have undergone α-cleavage to generate *n*-tridecane (n-C_{13}). n-C_{13} alkane was not detected in sample extracts, but its presence in the irradiated samples was confirmed by pyrolysis-GCMS, as described in Section 3.6. n-C_{13} alkane was susceptible to volatilization during extraction. If it had been retained, the GCMS analyses of extracts would have detected its presence based on comparison to alkane standards.

n-Hexacosane (n-C_{26} alkane) was confirmed to be present in the 1 and 2 MGy samples based on mass spectral match to the NIST 08 reference library and by retention time compared to an alkane reference mixture (Supplementary Figs. S2, S3, and S4). n-C_{26} alkane was also detected in the 0.2–0.5 MGy samples, but its presence could only be determined

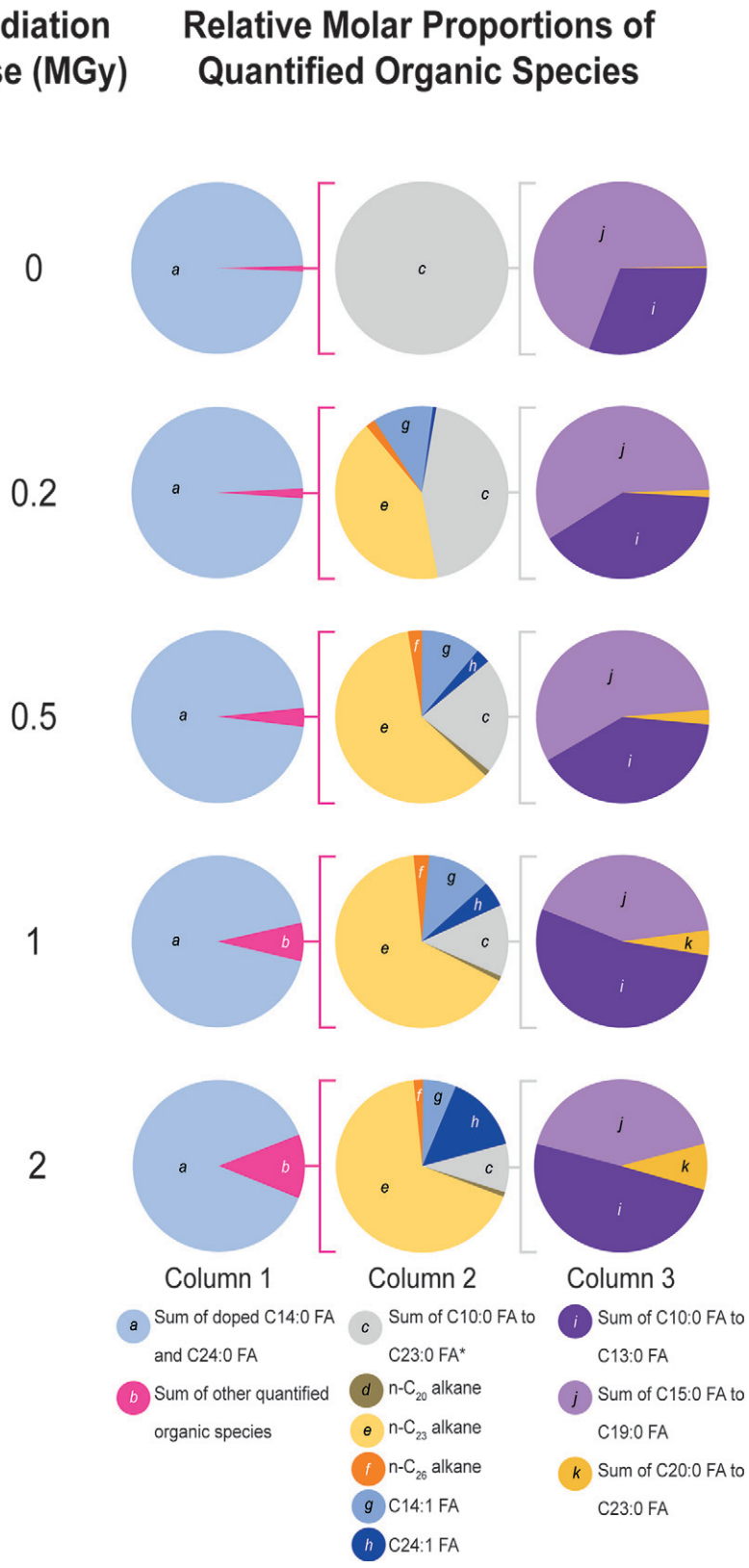

FIG. 1. Relative molar proportions of quantifiable organic species detected in solvent extracts from the control and irradiated samples. Column 1 indicates the proportion of total doped C14:0 FA and C24:0 FA to total non-doped quantifiable organic species. Column 2 shows the relative proportions of the non-doped quantifiable organic species to each other. Column 3 indicates how the population of non-doped saturated fatty acids changed with radiation dose. *Sum of C10:0 FA to C23:0 FA does not include the doped C14:0 FA. C14:0 FA, tetradecanoic acid; C24:0 FA, tetracosanoic acid.

Table 1. Concentrations by Mass of Organic Species Detected in Control and Irradiated Samples (Ppm)

	Radiation Dose				
Compound	*0*	*0.2*	*0.5*	*1*	*2*
Concentrations of N-Alkanes Detected					
N-C_{20}[a]	N.D.	N.D.	0.09 ± 0.02	0.16 ± 0.07	0.25 ± 0.07
N-C_{23}	N.D.	1.71 ± 0.96	5.29 ± 0.90	12.98 ± 5.06	21.68 ± 6.58
N-C_{26}[a]	N.D.	0.08 ± 0.02	0.26 ± 0.07	0.64 ± 0.14	0.64 ± 0.19
Concentrations of Monounsaturated Fatty Acids Detected					
C14:1	N.D.	0.32 ± 0.10	0.68 ± 0.18	1.66 ± 0.21	1.39 ± 0.22
C24:1	N.D.	0.03 ± 0.03	0.27 ± 0.12	1.06 ± 0.69	5.27 ± 2.93
Concentrations of Non-Doped Saturated Fatty Acids Detected					
Sum of C10:0 — C13:0	0.70 ± 0.51	0.44 ± 0.12	0.47 ± 0.09	0.86 ± 0.16	0.87 ± 0.21
Sum of C15:0 — C19:0	2.17 ± 1.52	0.86 ± 0.17	0.88 ± 0.31	0.90 ± 0.28	0.98 ± 0.27
Sum of C20:0 — C23:0	0.01 ± 0.02	0.02 ± 0.01	0.05 ± 0.03	0.11 ± 0.05	0.20 ± 0.11
Concentrations of Doped Saturated Fatty Acids Detected					
C14:0	147.38 ± 19.53	118.13 ± 28.22	105.27 ± 20.19	103.24 ± 5.75	63.51 ± 4.91
C24:0	156.41 ± 88.53	56.39 ± 45.49	102.54 ± 65.19	121.29 ± 45.41	163.93 ± 32.72

[a]Concentrations for n-C_{20} and n-C_{26} alkanes estimated using n-C_{23} alkane calibration curve. N.D., indicates no detection.

based on retention time. There was no detection of C27:0 FA in any extract, so it was concluded that n-C_{26} alkane was formed by the combination of n-C_{13} alkane fragments produced by the radiolysis of C14:0 FA. Hau and Nawar (1986) observed radiolysis products combining in their study of fatty acid monolayers. Here, this process would have been favored by the relatively high starting concentration of C14:0 FA and its deposition onto a solid salt surface. The n-C_{23} alkane calibration curve was used to estimate the abundance of n-C_{26} alkane in the 1 and 2 MGy samples, which was found to be ~0.6 ppm. Minor peaks with mass spectra and retention times consistent with n-C_{20} alkane were also detected in the irradiated samples, which indicates that small amounts of other chain length saturated hydrocarbons were being formed (Supplementary Figs. S4, S5, and S6).

3.1.2. Monounsaturated fatty acids. C14:1 FA and C24:1 FA made up a significant proportion of the non-doped organic species detected in extracts from the irradiated samples (Table 1; Fig. 1, Column 2). Due to their absence in the control, C14:1 FA and C24:1 FA were interpreted to be radiation products, but their detection was unexpected as unsaturated fatty acids are not typically listed as major products in published studies of fatty acid radiolysis. Alkenes are the unsaturated species most commonly reported in these works (e.g., Dubravcic and Nawar, 1976; Kim *et al*., 2004).

C14:1 FA showed a clear increase in abundance with radiation dose up to 1 MGy in our samples. At 2 MGy, the mean concentration of C14:1 FA was slightly lower than at 1 MGy. The concentration of C24:1 FA increased with radiation dose up to the maximum of 2 MGy. C18:1 FA was detected in extracts from the 2 MGy sample, which indicates that radiation was forming detectable concentrations of unsaturated fatty acids from saturated fatty acids in the sample background and not just the doped species.

3.1.3. Additional combined radiolysis products and alkenes. The focus of this study was to identify the most readily detectable organic products of the radiolysis of saturated fatty acids. While the alkanes and monounsaturated fatty acids described in Sections 3.1.1–3.1.2 produced clear quantifiable peaks, there were a multitude of small peaks in the chromatograms that were close to background and, thus, challenging to conclusively identify. These organic species were identified as radiation products only if they were detected in multiple samples at a particular radiation dose, if they exhibited an excellent match with reference library mass spectra, and if the species were absent in the controls. If a reference library mass spectrum was not available, the structure was deduced by *de novo* interpretation of the mass spectrum.

The results described in Section 3.1.1 indicate that some of the n-C_{13} alkane formed by the radiolysis of C14:0 FA had combined to produce n-C_{26} alkane. Two additional organic species were identified in the irradiated samples that further indicate a portion of the n-C_{13} alkane radiolysis products were combining with other radiolysis products to produce compounds with greater molecular masses than the starting fatty acids. The first compound was a ketone, which was identified as 14-heptacosanone ($C_{27}H_{57}O$), based on a match with the NIST 08 library reference spectrum (Supplementary Figs. S7 and S8). The second compound was an ether, which was interpreted to be hexadecyl tridecyl ether ($C_{29}H_{60}O$) based on the fragmentation pattern (Supplementary Figs. S9 and S10).

The results described in Section 3.1.2 indicate that gamma radiation was generating unsaturation in both doped and background fatty acids, which is consistent with the work of Dole *et al*. (1958). A small peak that eluted just before n-C_{23} alkane in the chromatograms of extracts from the irradiated samples was confirmed to be *n*-tricosene (n-C_{23} alkene) (Supplementary Figs. S11 and S12). The location of the n-C_{23} alkene double bond could not be determined with sufficient confidence due to the n-C_{23} alkene peak being present on the lower slope of the much larger n-C_{23} alkane peak.

3.2. The response of salt-bound saturated fatty acids to gamma radiation

A substantial decrease in C14:0 FA concentration was observed in the 0.2 MGy sample compared to the non-

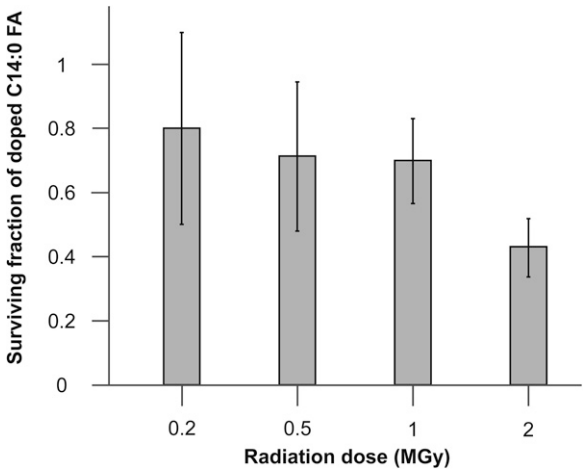

FIG. 2. The surviving fraction of C14:0 FA detected in the $MgSO_4 \cdot H_2O$ powders at each radiation dose relative to the C14:0 FA concentration measured in the non-irradiated control. C14:0 FA, tetradecanoic acid; $MgSO_4 \cdot H_2O$, magnesium sulfate monohydrate.

irradiated control (Table 1; Fig. 2; Supplementary Table S3). There was also a notable increase in aliquot-to-aliquot variability, with the mean C14:0 FA surviving fraction measured to be 0.80 (±0.30) of the control. C14:0 FA concentrations and sample heterogeneity were both found to decrease at higher radiation doses. The surviving fractions calculated for the 0.5 and 1 MGy samples were 0.71 (±0.23) and 0.70 (±0.13) of the control, and after a 2 MGy dose, only 0.43 (±0.09) of the starting fatty acid concentration remained. The decrease in C14:0 FA concentration equated to a radiolysis constant of 0.426 ± 0.043, which indicates a 50% loss of starting C14:0 FA after a 1.627 ± 0.164 MGy dose. For C24:0 FA, there was no clear decrease in abundance with increasing radiation dose, and the calculated error was high (Table 1). The mean C24:0 FA concentration for the 2 MGy sample was, in fact, slightly higher than that measured in the control. Substantial sample heterogeneity and poor methylation efficiency for C24:0 FA, due to its chain length, were suspected.

If it is assumed that all the fatty acids added to the rotary evaporator during sample preparation were deposited on the $MgSO_4 \cdot H_2O$ powder and that the solvent extraction and methylation steps had a 100% yield, the concentrations by mass for each fatty acid would have been ~2,700 ppm in the non-irradiated control. Instead, the calculated concentrations were on the order of 100–200 ppm for both fatty acids (Table 1).

It was inferred that most of the fatty acids present in the rotary evaporator during sample preparation were precipitated onto the sides of the flask rather than the $MgSO_4 \cdot H_2O$ powder. A DCM-methanol rinse of the rotary evaporator flask after the synthesis and removal of a sulfate-fatty-acid mixture indicated the presence of a residual fatty acid population bound to the flask that could be extracted with DCM-methanol but not DCM only (Supplementary Fig. S13). The GCMS analyses of three 10 mg aliquots from each sample powder indicated that C14:0 FA had precipitated onto the $MgSO_4 \cdot H_2O$ homogenously, but the C24:0 FA was distributed extremely heterogeneously, which was likely due to the C24:0 FA precipitating rapidly from solution. Due to these findings, only C14:0 FA is shown in Figure 2, and no radiolysis constant was calculated for C24:0 FA.

It is possible that a portion of the C14:0 FA and C24:0 FA mixed with $MgSO_4 \cdot H_2O$ may not have been readily recoverable by DCM extraction, so thermal extraction was used to further characterize the fatty acid compositions of the sample powders. The EGA-MS and pyrolysis-GCMS results described in Sections 3.5 and 3.6 show two distinct releases of organic fragments during heating, which suggests two different associations between the fatty acids and the $MgSO_4 \cdot H_2O$ surface. Both populations showed substantial losses with radiation.

Prior studies have noted that long-chain fatty acids are more resistant to methylation than shorter chains (Gries *et al.*, 2021). TMSH reaction efficiency was established to not be a major source of error in this present work; aliquots of the control and 2 MGy mixtures were sampled using the optimized TMSH method described in Section 2.3, and the C14:0 FA concentrations obtained were similar to those of the standard methylation method (Supplementary Table S4). The C24:0 FA detections were also consistent with those of the standard methylation method.

In addition to the doped C14:0 FA and C24:0 FA, trace amounts of other saturated fatty acids were detected. Given the low abundances of these non-doped fatty acids, they were grouped by carbon number range to more clearly examine how the relative proportions of non-doped fatty acid chain lengths changed with radiation dose (Table 1; Fig. 1, Column 3). The C10:0 FA–C13:0 FA group represented shorter-chain fatty acids potentially formed by C14:0 FA decomposition. The C15:0 FA–C19:0 FA group indicated minor background fatty acid contaminants, which are typically dominated by bacterial and eukaryotic C16:0 FA and C18:0 FA (e.g., Georgiou and Deamer, 2014; Summons *et al.*, 2008). The C20:0 FA–C23:0 FA group reflected shorter-chain fatty acids potentially formed by C24:0 FA decomposition.

In the non-irradiated control, saturated fatty acids comprised all the non-doped organic species quantified. The C15:0 FA–C19:0 FA group made up the greatest relative molar proportion of the three groups, as expected from minor background contamination. Groups 1 and 3 made up 31% and 0.3%, respectively, and likely reflected other contaminants in the doped species. In contrast, saturated fatty acids made up less than half of the non-doped population in the 0.2 MGy sample, due to the production of abundant alkane and unsaturated fatty acid radiolysis products (Sections 3.1.1 and 3.1.2). The relative molar proportions of Group 1 and 3 both increased dramatically after irradiation. In the 2 MGy sample, Group 1 comprised 50% of the non-doped saturated fatty acid population, and Group 3 made up 9%. These observations indicated that gamma radiolysis of saturated fatty acids on $MgSO_4 \cdot H_2O$ resulted in the production of shorter-chain saturated fatty acids.

Closer examination of the fatty acids that comprised Group 3 suggested a substantial increase in the estimated yield of C21:0 FA with increasing dosage compared to other Group 3 fatty acids, which was particularly striking as there was no detection of C21:0 FA in the non-irradiated control, while C20:0 FA, C22:0 FA, and C23:0 FA were present at low background concentrations. However, high uncertainties (equivalent to the low concentrations of the C20:0 FA–C23:0 FA

products and the heterogeneity of the parent C24:0 FA) challenged further interpretations beyond that shown for group summations in Figure 1.

3.3. Raman spectroscopy

Strong Raman $MgSO_4$ peaks dominated the spectra in each sample (Table 2; Fig. 3a), with some variation in peak position due to changes in hydration state (as observed by peak shifts of the ν_1SO_4 bands $\sim$989 cm^{-1} and 1050 cm^{-1} and the higher frequency hydration bands $\sim$3200–3440 cm^{-1} (Wang *et al*. 2006). This was not surprising, since $MgSO_4$ is known to readily change hydration state (Roach *et al*. 2009).

The doped fatty acids were infrequently observed as low intensity peaks in each of the samples. A correlation between radiation dose and the number of fatty acid Raman peaks observed could not be made. Interestingly, more of the original doped fatty acid peaks were observed in the 0.2 MGy and 2 MGy samples in comparison to the control and 0.5 MGy and 1 MGy samples. This could be due to the peak intensities of the $MgSO_4{\cdot}H_2O$, which were much stronger than the fatty acid peaks in general, as well as the main SO_4 peak positions 989 cm^{-1}, $\sim$1050 cm^{-1}, 1120 cm^{-1}, and 1220 cm^{-1} that overlap with some of the expected fatty acid peaks (Supplementary Fig. S14).

Multiple measurements of different spots on each sample were necessary to detect the fatty acids, which suggests that they were distributed non-uniformly on the $MgSO_4{\cdot}H_2O$ surfaces at Raman focal point scales. Similar issues have been documented by other researchers in which sample heterogeneity was cited as the main challenge in detecting organic molecules (Culka *et al*. 2019). Discernment between C14:0 FA and C24:0 FA was also not straightforward due to the weakness of their Raman peaks. Figure 3b shows some of the lower frequency vibrational modes (100–420 cm-1) related to longitudinal acoustic mode (LAM) frequencies of the fatty acid

Table 2. Raman Peak Shifts for MgSO4·H2O, Doped Fatty Acids, and Radiolysis Products

	Radiation Dose (MGy)				
Vibrational Mode (cm^{-1})	*0*	*0.2*	*0.5*	*1*	*2*
$MgSO_4$					
Mg-SO_4	206	212	219		
SO_4				255	
n_2SO_4	440	438	439	441	438
n_2SO_4	486	484	486	499	
n_4SO_4	635	632	635	634	
n_1SO_4 (OH)			989	989	
n_1SO_4	1052	1050	1052	1053	
n_3SO_4	1118	1118	1121	1118	
n_3SO_4		1217	1216	1222	
SO_4 bending mode	1512w[a]	1511	1507		
SO_4 bending mode				1643	
SO_4-H_2O	3203	3222	3229		
SO_4-H_2O	3271				
SO_4-H_2O	3349	3358	3326		
SO_4-H_2O	3443				
Doped Fatty Acids					
C = C	108	108	115	108	
C = C	279	272	275		
C-O-O (C14:0 FA)	866	873			
C-C				1060	1060
CH_2	1125				
CH_2					1417
CH_2-CH_3		1442		1441	1435
CH_2-CH_3	1463	1463			1463
Carboxylic Acid (OH)					2720
$n_s(=CH_2)$		2857			2842
$n_{as}(=CH_2)$		2884			2877
$n_s(=CH_3)$	2899w[a]	2902	2915w-br[a]		2919
$n_{as}(=CH_3)$		2933			
Radiolysis Products					
Branched alkane				828	
N-C_{23} alkane				1167	
N-C_{23} alkane					1290
CH_3 (aliphatic)				1347	
OCH_3-OCH_2 (alkane)				1488	
C = C		1550			
C = O				1757	
OH (carboxylic acid)	3156				

[a]w, weak; br, broad.

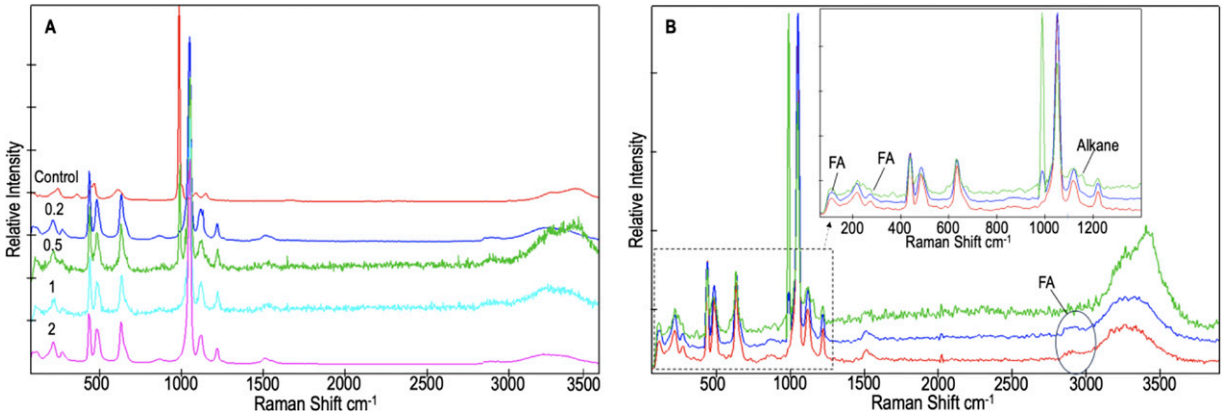

FIG. 3. **(A)** Representative Raman spectra from each sample set, the non-irradiated control (red), 0.2 MGy (blue), 0.5 MGy (green), 1 MGy (teal), and 2 MGy (pink). In all cases the fatty acid peaks were not readily discernible among the strong $MgSO_4{\cdot}H_2O$ peaks. **(B).** Raman spectra collected from the control (red), 0.5 MGy sample (blue), and 1 MGy sample (green) showing distinct $MgSO_4{\cdot}H_2O$ peaks between ~210 cm^{-1} and 1510 cm^{-1}, broad $MgSO_4{\cdot}H_2O$ hydration peaks between ~3200 cm^{-1} and 3450 cm^{-1}, weaker fatty acid peaks dominated by C14:0 FA (inset) and broad/weak fatty acid peaks between ~2850 cm^{-1} and 2940 cm^{-1} (circled). Inset shows a close-up of the lower end of the spectrum highlighting the presence of the C14:0 FA peaks ~110 cm^{-1} and 275 cm^{-1} in each spectrum along with an n-C_{23} alkane peak ~1167 cm^{-1} in the 1 MGy sample. C14:0 FA, tetradecanoic acid; $MgSO_4{\cdot}H_2O$, magnesium sulfate monohydrate.

chains that were observed in our samples. These LAM frequencies mostly correlated with literature values for C24:0 FA, but the same values (~ 110 cm-1 and 270 cm-1) were observed in our C14:0 FA standard (Minoni *et al*. 1984; Warren and Hooper 1973). Despite the overlaps between most of the organic peaks (Supplementary Fig. S14), evidence of n-C_{23} alkane was observed by two peaks in the 1MGy samples ~828 cm-1 and 1488 cm-1 and in the 2MGy samples ~1167 cm-1 and 1290 cm-1 (Blázquez-Blázquez *et al*. 2020). This radiolysis product was observed most readily in the 1MGy samples (Table 2).

3.4. Laser desorption and ionization mass spectrometry

Figure 4 shows representative negative ion mass spectra for the non-irradiated control and irradiated mixtures. The deprotonated C14:0 FA was consistently detectable across all radiation doses, but deprotonated C24:0 FA was only observable in the 0–1 MGy samples and not detected in the 2 MGy sample. Furthermore, C15:0 FA to C22:0 FA fragments were also present in the spectra, with no significant differences among samples irradiated from 0 to 1 MGy. However, as the radiation dose increased to 2 MGy, the relative intensity of C20:0 FA to C22:0 FA became more pronounced. LDI-MS observations of C24:0 FA and saturated fatty acids of Group 3 (C20:0 FA to C23:0 FA) were consistent with the GCMS observations, corroborating the notion that a fraction of the doped C24:0 FA decomposed into shorter-chain fatty acids under gamma radiation. However, it is important to note that LDI-MS peak intensities can be impacted by several factors other than analyte abundance, such as sample morphology, ionization efficiency, and the electronic structures of clusters. In addition, LDI-MS is a surface analysis technique, while GC-MS examined extracts from bulk samples.

In the LDI-MS data, there was no clear evidence of the major alkane and unsaturated fatty acid products detected through GCMS and Raman spectroscopy. One plausible explanation for the absence of these organics or their clusters in the LDI-MS results is that the quantities generated during the experiment were below the detection threshold of LDI-MS. Particularly in the case of volatile species, within the high vacuum environment of LDI-MS, the concentrations may have been insufficient for reliable detection and characterization. The LDI-MS results for a pure n-C23 alkane standard are shown in Supplementary Figure S15 as a reference, where fragment peaks were detected in the positive mode but not in the negative mode.

3.5. Evolved gas analysis mass spectrometry

EGA-MS was used to provide a broad characterization of the inorganic and organic compositions of the control and 0.5–2 MGy samples immediately after opening of the cryogenic ampules (Fig. 5). The maximum of the pyrolysis temperature ramp was set below the thermal decomposition temperature of anhydrous $MgSO_4$ (Scheidema and Taskinen, 2011), but two broad SO_2 peaks were still produced by each sample at 350°C and 700°C. Releases of CO_2, COS, and CS_2 were associated with these SO_2 evolutions, and the 350°C releases became somewhat stronger during heating of the irradiated samples compared to the control (Supplementary Fig. S16). The 350°C releases also coincided with a large H_2O peak that indicated dehydration of the $MgSO_4{\cdot}H_2O$. Interestingly, this H_2O peak was broader and occurred at a slightly higher temperature than the dehydration peak observed for pure $MgSO_4{\cdot}H_2O$ (Supplementary Fig. S17a). The 350°C SO_2 peak developed a minor low-temperature shoulder after a radiation dose of 0.5 MGy, which became more pronounced at higher doses. The substantial releases of CO_2 that accompanied the 700°C SO_2 peaks were interpreted to be the result of the thermal decomposition of carboxylic acid functionalities adsorbed onto the sulfate surface. The presence of fatty acids and their volatile radiolysis products in the irradiated samples caused partial thermal decomposition of the $MgSO_4$ at significantly lower temperatures than observed for the pure sulfate phase.

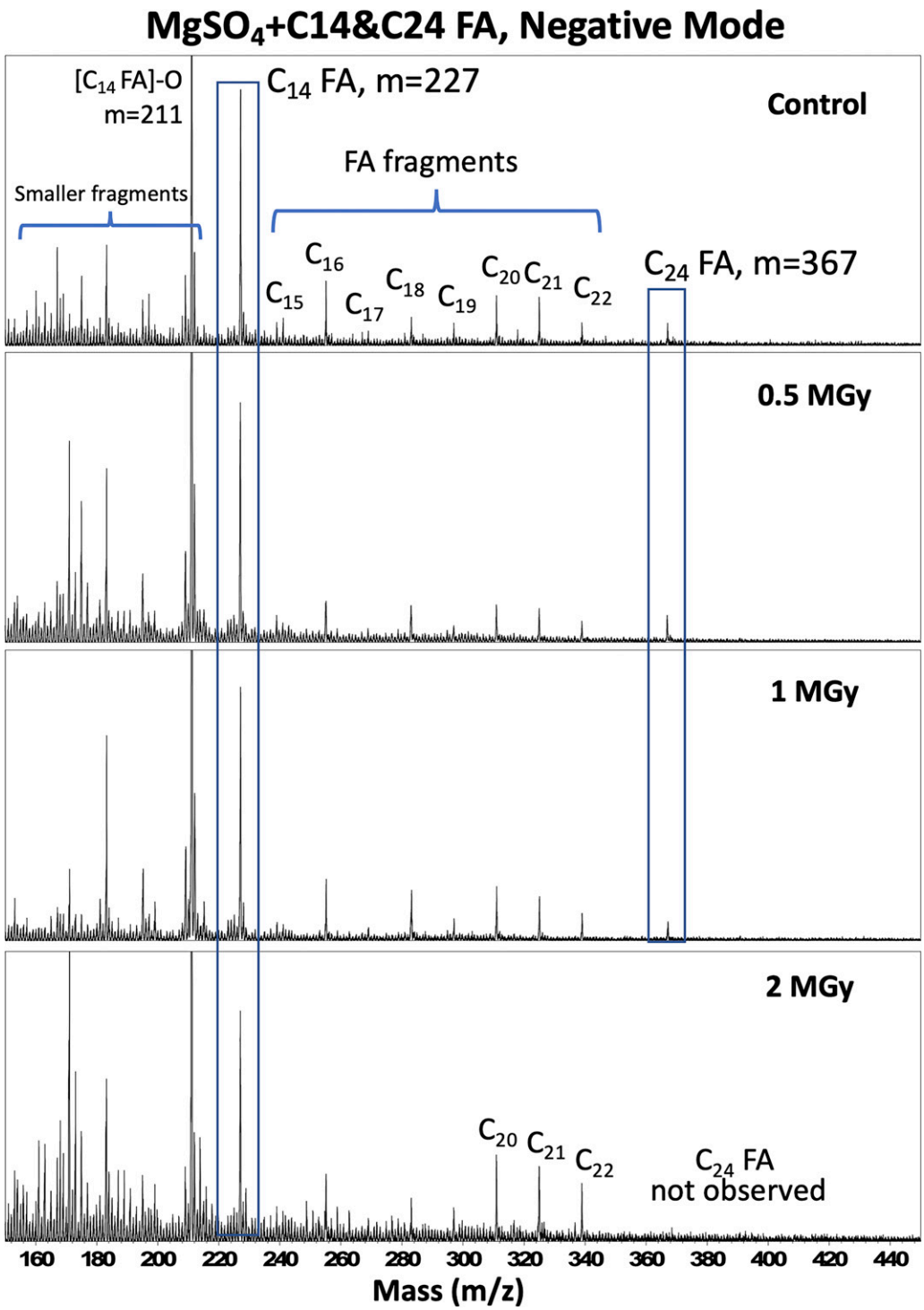

FIG. 4. Mass spectral results obtained through LDI-MS in the negative mode for the non-irradiated control and irradiated samples. The highlighted peaks correspond to the detection of the deprotonated fatty acids for C14:0 FA at *m/z* 227 and C24:0 FA at *m/z* 367. C15:0 FA to C22:0 FA fragments peaks are also highlighted. C14:0 FA, tetradecanoic acid; C24:0 FA, tetracosanoic acid; LDI-MS, laser desorption and ionization mass spectrometry.

The control mixture produced two major peaks of hydrocarbon fragments at 375°C and 475°C during EGA-MS [representative mass to charge ratios (*m/z*) 41, 43, 55, 57, 69, 71, 83, 85 are shown in Fig. 5], which were interpreted to have been produced by pyrolysis of the doped fatty acids. Pure C14:0 FA was shown to decompose at 300°C in the EGA-MS system (Supplementary Fig. S17b). However, when an EGA-MS test was performed using a reference sample where C14:0 FA had been mixed with $MgSO_4$ as the sulfate precipitated from aqueous solution, the major release of hydrocarbon fragments was not observed until 520°C, along with a pronounced lower-temperature shoulder that peaked at ~400°C

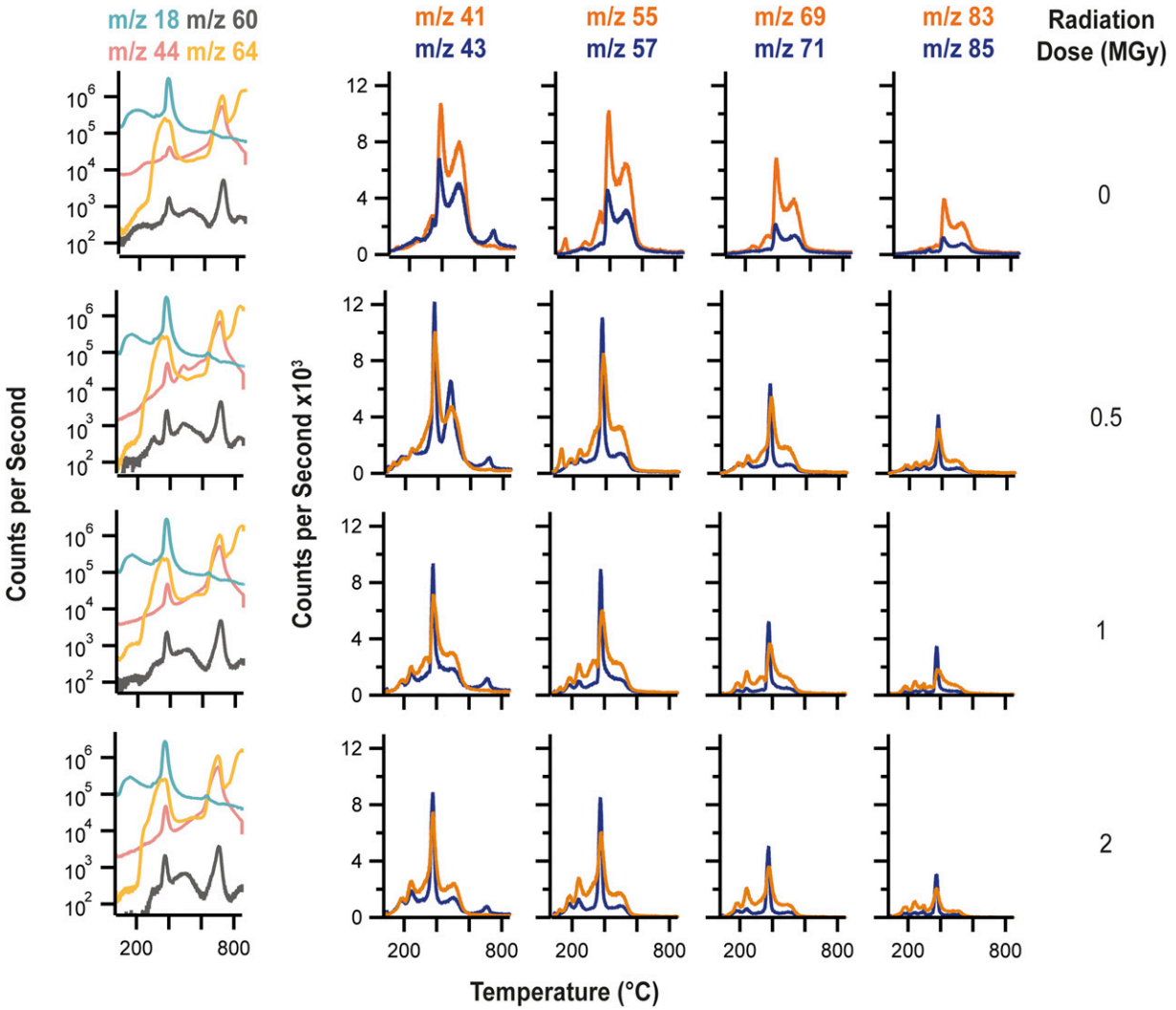

FIG. 5. EGA-MS plots showing major gases and organic fragments detected during heating of the non-irradiated control and 0.5–2 MGy samples. The left-hand column shows the evolutions of H_2O (*m/z* 18), CO_2 (*m/z* 44), COS (*m/z* 60), and SO_2 (*m/z* 64). CS_2 was also detected but is not shown in these plots, as its EGA-traces overlapped with those of COS (Supplementary Fig. S16). The four columns to the right show representative organic fragments detected during EGA-MS. These masses were selected to demonstrate the temperatures at which organic fragments were being liberated from the samples and the relative proportions of alkyl fragments (*m/z* 43, 57, 71, 85) compared to alkenyl fragments (*m/z* 41, 55, 69, 83), which informed about the presence of unsaturation in the pyrolysis products. EGA-MS, evolved gas analysis mass spectrometry.

(Supplementary Fig. S17c). An additional EGA-MS test using a reference sample that consisted of C12:0 FA and C14:0 FA mixed with $MgSO_4$ as it precipitated from aqueous solution produced a similar array of hydrocarbon fragments at ~400°C and 520°C (Supplementary Fig. S17d). These tests confirmed that deposition of fatty acids onto $MgSO_4$ significantly changed their behavior during EGA-MS, such that they became more resistant to desorption and pyrolysis, as indicated by higher release temperatures for organic fragments. Distinguishing the chain lengths of doped fatty acids in such samples with EGA-MS data is not possible. Therefore, while the EGA-MS results of the non-irradiated control were consistent with the presence of fatty acids, it was not clear that the 375°C and 475°C releases of hydrocarbon fragments corresponded to C14:0 FA and C24:0 FA, respectively. It is instead concluded that both fatty acids may have contributed fragments at 375°C and 475°C and that the separate release temperatures were governed by two different associations between the fatty acids and the $MgSO_4{\cdot}H_2O$ powder, which led to two different thermal release processes. The fact that the lower temperature release coincided with dehydration of the $MgSO_4{\cdot}H_2O$ suggests that water was involved in adsorbing the fatty acids fragmented at this temperature. The 475°C release of organic fragments was suggestive of pyrolysis occurring in the alkyl chains of fatty acids strongly bound to $MgSO_4{\cdot}H_2O$ surfaces, as supported by the pyrolysis-GCMS data (Section 3.6).

Further evidence that the deposition of C14:0 FA and C24:0 FA onto $MgSO_4{\cdot}H_2O$ significantly altered their thermal behavior was revealed by examining the EGA-MS traces for fragments from the carboxylic acid head group (*m/z* 73, 60, 129) and the relative intensities of alkyl fragments (*m/z* 43, 57, 71, 85) compared to alkenyl fragments (*m/z* 41, 55, 69, 83) from

the fatty acid hydrocarbon tail (Supplementary Figs. S16 and S17). In contrast to EGA-MS of pure C14:0 FA, where the fatty acid was likely readily volatilized and then fragmented in the EI source of the MS, no major peaks for *m/z* 73, 60, and 129 that could be clearly attributed to C14:0 FA were produced by the control and the irradiated samples. While pure C14:0 FA produced similar intensities of alkyl and alkenyl fragments during EGA-MS, in the control mixture the alkenyl fragments had greater intensities than the alkyl fragments. Stepped pyrolysis GCMS studies of aliquots of the control and 2 MGy samples were conducted to better understand the release of organic fragments during EGA-MS; the findings are reported in Section 3.6.

The irradiated samples generally produced similar intensity alkyl peaks at 375°C compared to alkenyl, with the slightly stronger alkyl peaks suggestive of alkanes (Fig. 5). The majority of hydrocarbon peaks detected at 475°C exhibited more intense peaks for alkenyl fragments, as was seen in the control, but all of the organic fragment peaks at this temperature were significantly weaker than was observed in the control. As the radiation dose increased, minor hydrocarbon peaks were detected at low temperatures (<300°C), which indicates the formation of volatile alkane radiolysis products.

3.6. Stepped pyrolysis gas chromatography mass spectrometry

Stepped pyrolysis GCMS experiments were conducted on aliquots of the non-irradiated control and 2 MGy samples to better understand the sources of organic fragments detected during EGA-MS (Section 3.5). Significant differences in hydrocarbon detections were observed between each of the three flash heating steps (200°C, 400°C, and 600°C) for both samples and radiolysis products that were previously identified or inferred via GCMS of solvent extracts were clearly distinguishable in the 2 MGy sample compared to the control (Fig. 6). The control sample heated to 200°C produced no major peaks, but minor signals detected towards the end of the chromatogram were indicative of species resulting from instrument carryover. At 400°C, the chromatogram was dominated by a single intense peak identified as C14:0 FA, indicating that when liberated from the dehydrating $MgSO_4{\cdot}H_2O$ at this temperature, C14:0 FA did not undergo any substantial pyrolytic fragmentation. No peaks indicative of intact C24:0 FA were detected. At 600°C, the control evolved a multitude of peaks including a series of C_9-C_{19} alkenes and lesser amounts of alkanes. The alkene series consisted of a distinctive repeating pattern, where four alkenes would be detected for the same carbon number, which suggests multiple isomers of each alkene pyrolysis product. C_{12}-alkene produced the most intense set of peaks, with the peak intensities decreasing as carbon number increased. Minor alkane peaks of the same carbon number were occasionally detected among the alkene peaks. The array of hydrocarbons observed in the 600°C chromatogram was similar to data presented in petroleum and biofuels studies where fatty acids underwent pyrolytic cleavage; that is, they were thermally "cracked" into hydrocarbons (e.g., Asomaning *et al*., 2014; de Morais Araújo *et al*., 2017; Freitas *et al*., 2019; Fréty *et al*., 2014; Maher *et al*., 2008; Snåre *et al*., 2006). Such works report the pyrolytic production of saturated and unsaturated hydrocarbons from adsorbed saturated fatty acids via decarboxylation and decarbonylation, respectively. Here, it is inferred that pyrolysis of adsorbed fatty acids was the primary source of the peaks detected at 600°C in the stepped pyrolysis GCMS experiments and at 475°C in the EGA-MS data. This process also appeared to be the source of organic fragments detected at 375°C during EGA-MS of the control, due to the relative proportions of the fragments indicating unsaturation, while the flash heating of the stepped-pyrolysis-GCMS technique liberated the intact C14:0 FA as the salt dehydrated at 375°C. Stepped pyrolysis GCMS of the pure $MgSO_4{\cdot}H_2O$ powder and $MgSO_4{\cdot}H_2O$ that had been mixed with DCM solvent and dried under N_2 confirmed that background contaminants in the sulfate and DCM were not the source of the alkenes and alkanes detected at 600°C in the non-irradiated control and 2 MGy sample (Supplementary Fig. S18).

The chromatograms produced by stepped pyrolysis of the 2 MGy sample at 200°C and 400°C were substantially different from those of the non-irradiated control. Sharp peaks for n-C_{13} alkane and n-C_{23} alkane were seen at both temperatures. C14:0 FA was still detected at 400°C, but the peak was much weaker than the alkane peaks and when compared to the C14:0 FA peak of the control. The contrast between the 2 MGy sample and control chromatograms at 200°C and 400°C clearly illustrated the alteration of the starting fatty acids to radiolysis products dominated by alkanes. The series of hydrocarbon chain lengths observed in the 600°C chromatogram of the 2 MGy sample were remarkably similar to those seen in the control. However, there was a substantial weakening of the alkene peaks, and alkanes were clearly detected for every carbon number from C_{11} to C_{21}. While the pyrolysis products of the non-irradiated control at 600°C were dominated by unsaturated hydrocarbons, the irradiated samples produced a more complex mixture of saturated and unsaturated hydrocarbon products.

The pyrolysis-GCMS results support the finding of the EGA-MS investigation that the fatty acids were present on the $MgSO_4{\cdot}H_2O$ surface in two distinct associations. One population was likely interfaced with the salt's structural water, and intact fatty acids were readily liberated from this pool by flash heating; the other fatty acid population was likely directly absorbed onto the sulfate surface, and thermal fragmentation occurred in the hydrocarbon tails of these fatty acids, followed by a higher-temperature CO_2 release as remaining absorbed carboxylic acid groups decomposed. It is possible that the two fatty acid populations may have differed in how readily extractable they were with DCM, but substantial decreases in abundance and evidence of alteration were seen in the EGA-MS peaks for both fatty acid populations in the irradiated samples compared to the control, and for C14:0 FA in the pyrolysis GCMS chromatograms, indicating that regardless of which surface association the fatty acids were in, they were rapidly destroyed by gamma radiation.

4. Discussion

The exposure of a simple synthetic mixture consisting of $MgSO_4{\cdot}H_2O$ doped with C14:0 FA and C24:0 FA to gamma-ray doses of 0.2–2 MGy at −196°C yielded irradiated samples that hosted remarkably diverse inventories of organic radiolysis products (Fig. 7). While the presence of abundant C_{n-1} alkanes formed by α-cleavage of the starting fatty acids was consistent with existing literature on the

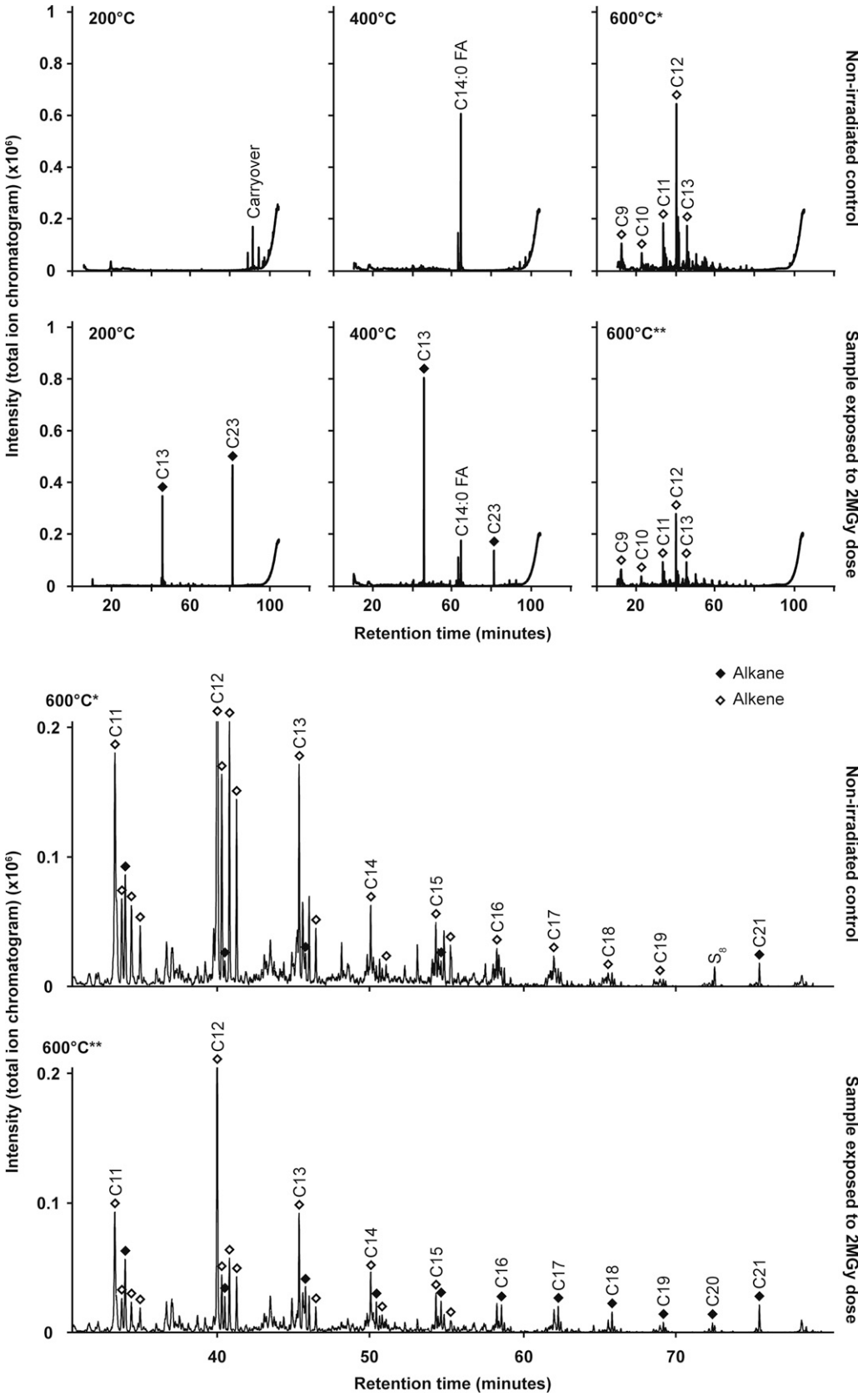

FIG. 6. Stepped pyrolysis GCMS plots for the non-irradiated control and 2 MGy sample. Chromatograms are shown for the 200°C, 400°C, and 600°C heating steps, and the major fatty acid, alkane (closed diamond), and alkene (open diamond) peaks are labeled along with their carbon numbers. *The 600°C chromatogram for the non-irradiated control is replotted below the stepped chromatograms at a larger scale and with the y-axis truncated at a signal intensity of 0.2×10^6 to show the series of alkene and alkane peaks more clearly. **The 600°C chromatogram for the 2 MGy sample is presented at the same larger scale. Note that for both larger plots the strong C_{12} alkene peak is truncated. GCMS, gas chromatography mass spectrometry.

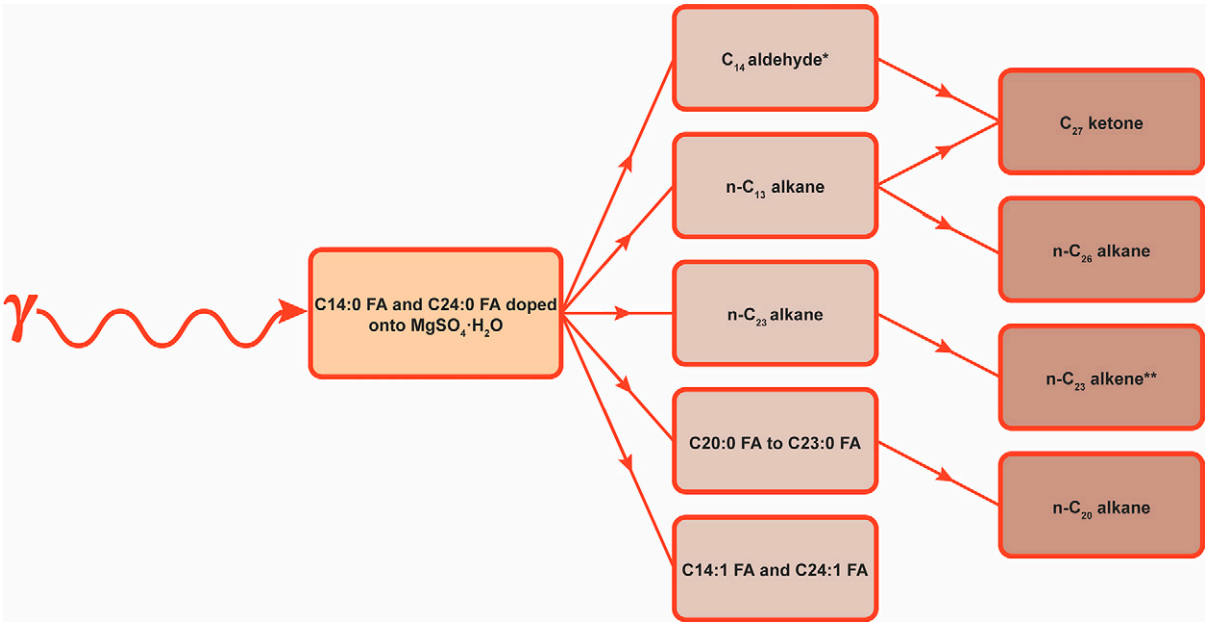

FIG. 7. Organic products formed by Europa-like gamma radiolysis of C14:0 FA and C24:0 FA doped onto $MgSO_4 \cdot H_2O$. The fatty acids were initially transformed into aldehydes, C_{n-1} alkanes, shorter-chain saturated fatty acids, and unsaturated fatty acids. Detections of a C_{27} ketone and C_{26} alkane were interpreted to be due to a fraction of the initial aldehyde and alkane products reacting. Gamma radiation is inferred to have induced unsaturation in a small proportion of the abundant n-C_{23} alkane product to form n-C_{23} alkene. The presence of an n-C_{20} alkane in 0.5–2 MGy samples was ascribed to α-cleavage of the shorter-chain saturated fatty acid products. *Aldehydes were not detected directly in the GCMS data but were interpreted to have been one of the parent compounds of the C_{27} ketone. **It is possible that n-C_{23} alkene could also have been formed by cleavage of the C24:1 FA radiolysis product. C14:0 FA, tetradecanoic acid; C24:0 FA, tetracosanoic acid; GCMS, gas chromatography mass spectrometry.

gamma irradiation of fatty acids (Supplementary Fig. S1) (Dubravcic and Nawar, 1968; 1976; Kim *et al*., 2004; Nawar, 1978; Vajdi *et al*., 1978; Wu and Howton, 1975), detections of unsaturated fatty acids, combined radiolysis products, and shorter-chain saturated fatty acids were attributed to the novel experimental parameters used in this study.

Unsaturated fatty acids of the same chain length as the doped fatty acids were the most abundant radiolysis products after C_{n-1} alkanes under the experimental conditions of this investigation. Dole *et al*. (1958) observed gamma rays inducing unsaturation in polyethylene and proposed that the double bonds were formed in the process of neutralizing ions produced by ionizing radiation. The high gamma ray doses used in this work likely generated a substantial proportion of unsaturated fatty acids via a similar process. The radiolysis of unsaturated fatty acids is more complex than for saturated fatty acids, as radiation-induced cleavage can preferentially occur at double bond sites in addition to near the carbonyl group (Dubravcic and Nawar, 1968; Vajdi *et al*., 1978); it is inferred that the ultra-low temperature of the radiation chamber may have slowed the destruction rate of the unsaturated fatty acids. Alkenes are the unsaturated species most commonly reported in existing radiolysis studies conducted under more standard conditions (e.g., Dubravcic and Nawar, 1976; Kim *et al*., 2004). In this work, a n-C_{23} alkene was detected at all radiation doses, but the corresponding chromatogram peak was significantly weaker than those of the unsaturated fatty acids. These results highlight the importance of conducting radiation investigations with experimental conditions that closely match the environment of interest. For planetary studies, any changes in the analog matrix, chamber temperature, radiation type, and radiation dosage would likely significantly impact results.

Irradiating relatively high concentrations of fatty acids precipitated onto a solid salt surface resulted in some of their radiolysis products combining to form particularly high-mass compounds. For example, n-C_{13} alkane, formed by α-cleavage of the doped C14:0 FA, and hexadecanal, formed by irradiation of background C16:0 FA, likely reacted to form hexadecyl tridecyl ether. Though aldehydes, such as hexadecanal, were not directly detected in this investigation, they are reported in many published fatty acid gamma radiolysis studies (Supplementary Fig. S1) (e.g., Dubravcic and Nawar, 1976; Nawar, 1978). Some of the n-C_{13} alkane radiolysis products combined with each other to form n-C_{26} alkane, while others reacted with the aldehyde produced by radiolysis of the starting C14:0 FA to form 14-heptacosanone. If n-C_{36} alkane and n-C_{46} alkane were formed by the combination of n-alkanes produced by radiolysis in this study, they would have escaped detection by the GCMS method employed.

The identification of shorter-chain saturated fatty acid products in the irradiated samples indicated that some of the doped C14:0 FA and C24:0 FA underwent a form of radiolytic fragmentation that differed from the predominant process of α-cleavage. Fatty acids in the range C20:0 FA to C23:0 FA were present at extremely low abundances in the non-irradiated control, but their concentrations increased substantially with increasing radiation dose (Table 1; Fig. 1).

This population in the irradiated samples was, therefore, interpreted to be composed primarily of radiolysis products rather than sample background. If the alkyl chain of the doped C24:0 FA had fragmented randomly under gamma radiation, the abundances of C20:0 FA to C23:0 FA in the irradiated samples would have been similar. However, the GCMS data suggest that C21:0 FA was a more abundant product than C20:0 FA, C22:0 FA, and C23:0 FA. It is suspected that C24:0 FA preferentially decomposed into C21:0 FA, but these observations should be treated with caution as due to the heterogeneity of the parent fatty acid and the weak GCMS signals of these minor radiolysis products, the estimates had extremely large quantitative uncertainties. If C21:0 FA was preferentially formed over other chain lengths, a potential mechanism was charge-remote fragmentation (CRF) that occurred when gamma rays deposited energy into doped fatty acids adsorbed onto the $MgSO_4{\cdot}H_2O$ surface. Analytical chemists use CRF to inform about the structures of long-chain compounds (Cheng and Gross, 2000; Jensen *et al*., 1985; Jensen and Gross, 1987). Typically, CRF is performed by generating a precursor ion via fast atom bombardment, which is then collision activated by an inert gas in the collision cell of a tandem mass spectrometer (Cheng and Gross, 2000; Jensen *et al*., 1985; Jensen and Gross, 1987). However, it is known that, if a compound with a long alkyl chain has its charge fixed at one end, and sufficient ionizing energy of any type is supplied, the compound will undergo CRF (Cheng and Gross, 2000). Investigations of the CRF of saturated fatty acids of ten carbons or higher show that C_3H_8 is the most abundant fragment lost from the hydrocarbon tail (Jensen *et al*., 1985). Here, it is hypothesized that CRF was induced in the adsorbed C24:0 FA by gamma radiation, which led to the preferential loss of a three-carbon fragment. This theory is supported by the detection of n-C_{20} alkane in the irradiated samples, which could have been sourced by α-cleavage of a relatively abundant C21:0 FA radiolysis product. Regardless of the molecular transformation type occurring, the results of this experiment indicate that radiolysis can induce changes in the distribution of fatty acid chain lengths. Radiation may erode both modal and patterned distributions within populations of fatty acids, potentially scrambling any abiological or biological information recorded by starting distributions.

The data indicate that gamma radiation rapidly destroyed C14:0 FA deposited on the surface of $MgSO_4{\cdot}H_2O$. The concentration of C14:0 FA in extracts from the 2 MGy sample was less than half that measured in extracts from the control. The calculated radiolysis constant of 0.426 ± 0.043 implies that $\sim$90% of the starting concentration of the fatty acid would be lost after $\sim$5 MGy of exposure and that fatty acids may be particularly challenging to detect in europan hydrated $MgSO_4$ deposits. For most locations on Europa, the upper millimeter of the crust will be subjected to $\sim$10 MGy dose in <1000 years (Nordheim *et al*., 2018). For materials at depths of $\sim$10 cm that are located in areas of Europa suspected to receive the lowest radiation dose rates, a 4 MGy dose will be reached within $\sim$13 million years (Pavlov *et al*., 2024). Our data can only quantitatively demonstrate rapid destruction of fatty acids that were readily extractable from $MgSO_4{\cdot}H_2O$ with DCM. The decomposition rate of any recalcitrant populations that were not DCM extractable is uncertain. However, the EGA-MS and pyrolysis GCMS results indicated all starting fatty acid populations in the samples experienced substantial deceases in abundance with radiation.

The results highlight the value of a multi-instrument approach when examining the organic chemistry of complex irradiated materials. While the GCMS analyses of solvent extracts from bulk 10 mg aliquots spearheaded the identification and quantification of the doped fatty acids and their major radiolysis products, the Raman spectroscopy, LDI-MS, EGA-MS, and pyrolysis GCMS investigations enabled rapid characterization of the samples, facilitated interpretations about highly volatile radiation products, and informed about associations between the fatty acids and $MgSO_4{\cdot}H_2O$ surfaces. The Raman analyses were challenged by the overlap between $MgSO_4$ and organic spectral features but were still able to identify fatty acids at every radiation dose, along with the alkanes and unsaturation produced by radiation, and evidence of branched products that were not identified in the GCMS data (Table 2). LDI-MS was able to readily identify C14:0 FA in every irradiated sample, and C24:0 FA could be identified in all mixtures, except for the 2 MGy sample. There was, however, a clear increase in the amount of small organic fragments and non-doped fatty acids detected by LDI-MS in the 2 MGy sample compared to the control.

EGA-MS provided a broad characterization of the organic and inorganic composition of the samples immediately after each cryogenic ampule was opened and revealed a complex set of interactions between the fatty acids and $MgSO_4{\cdot}H_2O$ that resulted in two discrete releases of organic fragments during ramped heating. Stepped-pyrolysis GCMS found that the control sample released intact C14:0 FA at 400°C and a series of alkenes and minor alkanes at 600°C. Comparison of the EGA-MS and pyrolysis-GCMS data suggests that the lower-temperature release of organic fragments was due to a portion of the doped fatty acids being adsorbed onto the $MgSO_4{\cdot}H_2O$ in a way that involved the salt's structural water. These fatty acids were liberated when the salt dehydrated, either because water was released or because of a change in the mineral structure when the water was lost. An important observation is that unlike pyrolysis-GCMS, EGA-MS, which uses ramped heating, did not yield readily detectable intact C14:0 FA at this temperature; instead, only hydrocarbon fragments cleaved from the fatty acid tail were observed. It therefore appears that, in certain situations, flash heating can liberate intact organic compounds via the dehydration of host minerals, which greatly assists in compound identification. Conversely, EGA-MS generates fragments that can inform about the presence and general nature of organic compounds and most critically their associations with different mineral phases. Identifying parent compounds in EGA-MS data can, however, be extremely challenging. The higher-temperature release of organic fragments seen during EGA-MS that was further studied with the 600°C pyrolysis-GCMS step was suggestive of a subset of the fatty acids being strongly absorbed onto the sulfate surface and undergoing "cracking" to release hydrocarbon fragments. Stepped pyrolysis GCMS of the 2 MGy sample at 200°C and 400°C demonstrated the production of abundant C_{n-1} alkanes by gamma radiolysis of the starting fatty acids. Radiation also led to an increase in the ratio of saturated to unsaturated hydrocarbon fragments released at 600°C.

The findings of this study have substantial implications for missions to Europa. If Europa's crustal dynamics were to

transport an organic-bearing hydrated magnesium sulfate deposit to the upper centimeters of the europan subsurface, where it would be exposed to extremely high radiation doses, any associated fatty acids would likely be rapidly destroyed. Much of these fatty acids would be expected to decompose into C_{n-1} alkanes, as is commonly reported in radiolysis studies of fatty acids (Dubravcic and Nawar, 1968; 1976; Kim *et al*., 2004; Nawar, 1978; Vajdi *et al*., 1978; Wu and Howton, 1975), but under the Europa-like parameters of this investigation, we also observed the formation of unsaturated fatty acids, high-mass combined radiolysis products, and shorter-chain saturated fatty acids. Prolonged exposure to radiation would likely result in radiolysis of the initial radiolysis products to generate multiple generations of radiolytically generated species. Thus, attempting to extract any information related to ocean chemistry and habitability potentially recorded by fatty acids present in irradiated sulfate deposits on Europa will be challenged by rapid loss of the initial fatty acid populations and the presence of diverse sets of complicating radiolysis products. While this study illustrated how the use of multiple complementary analytical techniques can help deconvolve organic signals in complex irradiated materials, any such signals are most likely to be detectable and interpretable in near-surface deposits on Europa that have been minimally irradiated.

Though magnesium sulfate deposits on Europa may be largely derived from surface radiation processes, it is possible that some units could be sourced from the subsurface, based on experimental (e.g., Fanale *et al*., 2001) and theoretical models of Europa's ocean chemistry (e.g., Zolotov and Shock, 2001). Potential delivery mechanisms for such units include melt-through of the crust from the ocean, diapirism, and cryovolcanism (Chivers *et al*., 2023). Regardless of their origins, any salts emplaced or generated within the upper few tens of centimeters of Europa's crust will be subsequently churned and mobilized by impacts (Costello *et al*., 2021). Given our limited understanding of how impact gardening and crustal dynamics will distribute salts on Europa, surface missions must be prepared for the potential presence of magnesium sulfate deposits at landing sites and the implications for the rapid transformation and destruction of any associated fatty acids by radiation.

5. Conclusions

When saturated fatty acids were precipitated onto $MgSO_4{\cdot}H_2O$ and exposed to gamma rays under Europa-like conditions, the major organic products were C_{n-1} alkanes, unsaturated fatty acids of the same chain length as the doped species, shorter chain-length saturated fatty acids, and a C_{n-1} alkene. Other products detected included high-mass alkanes, ethers, and ketones formed by the combination of radiolysis products. The surviving fraction of the starting fatty acids generally decreased significantly with radiation dose. Quantitation of fatty acid concentrations enabled the calculation of a radiolysis constant that indicated exposure to a 5 MGy dose of gamma radiation would have resulted in a $\sim$90% loss of the initial C14:0 FA population under these experimental conditions.

Interpretation of the complex organic chemistry of the irradiated materials was aided by utilizing multiple complementary analytical techniques. GCMS of methylated extracts from bulk samples enabled the identification and quantification of the starting fatty acids and most radiolysis products, while Raman spectroscopy and LDI-MS were able to examine the nature and distribution of these organic species on the $MgSO_4{\cdot}H_2O$ powder. EGA-MS indicated how the doped fatty acids comprised two distinct populations that had different associations with the $MgSO_4{\cdot}H_2O$ surfaces, which resulted in two discrete releases of organic fragments during heating. Stepped-pyrolysis-GCMS was able to liberate intact fatty acids from one of these populations via dehydration of the host $MgSO_4{\cdot}H_2O$ salt and was able to identify volatile C_{n-1} alkane products that were not readily detectable with other techniques.

Deducing the origins of europan fatty acids will be greatly challenged by the harsh radiation environment present at Europa's surface. In this study, when fatty acids were exposed to Europa-relevant gamma ray doses and temperatures, they rapidly decomposed to form diverse sets of radiolysis products. Such products may scramble and overprint residual starting fatty acid signals. Targeting near-surface deposits that have been minimally irradiated may still enable the detection of any surviving initial fatty acid signatures that could inform about the chemistry and habitability of Europa's subsurface crust and ocean.

Acknowledgments

The authors are grateful to Dr. Luoth Chou for providing supervision and feedback during the laboratory and article writing stages of this project. The authors are also appreciative for the support and guidance provided by Dr. Slávka Andrejkovičová and Mr. Brian Leiter during sample preparation.

Authors' Contributions

J.M.T.L.: Conceptualization, methodology, validation, formal analysis, investigation, writing—original draft, visualization, project administration, funding acquisition. D.M.B.: Conceptualization, formal analysis, investigation, writing—review and editing, visualization. A.A.P.: Conceptualization, methodology, formal analysis, writing—review and editing. X.L.: Conceptualization, formal analysis, investigation, writing—review and editing, visualization. S.Z.W.: Methodology, validation, investigation, writing—review and editing. J.L.E.: Conceptualization, methodology, validation, investigation, resources, writing—review and editing, supervision. A.C.M.: Conceptualization, writing—review and editing, supervision, project administration, funding acquisition.

Author Disclosure Statement

There are no competing financial interests for any of the authors.

Funding Information

Support for this research was provided by NASA's Planetary Science Division Research Program, through Internal Scientist Funding Model (ISFM) work package Fundamental Laboratory Research (FLaRe) at NASA Goddard Space Flight Center and by the Center for Research and Exploration in Space Science and Technology (CRESST) II Cooperative Agreement (NASA Award Number 80GSFC17M0002).

Supplementary Material

Supplementary Data S1
Supplementary Table S1
Supplementary Table S2

Supplementary Table S3
Supplementary Table S4
Supplementary Figure S1
Supplementary Figure S2
Supplementary Figure S3
Supplementary Figure S4
Supplementary Figure S5
Supplementary Figure S6
Supplementary Figure S7
Supplementary Figure S8
Supplementary Figure S9
Supplementary Figure S10
Supplementary Figure S11
Supplementary Figure S12
Supplementary Figure S13
Supplementary Figure S14
Supplementary Figure S15
Supplementary Figure S16
Supplementary Figure S17
Supplementary Figure S18

References

Ashkenazy Y. The surface temperature of Europa. *Heliyon* 2019;5(6):e01908; doi: 10.1016/j.heliyon.2019.e01908

Asomaning J, Mussone P, Bressler DC. Thermal cracking of free fatty acids in inert and light hydrocarbon gas atmospheres. *Fuel* 2014;126:250–255; doi: 10.1016/j.fuel.2014.02.069

Barge LM, Rodriguez LE, Weber JM, et al. Determining the "biosignature threshold" for life detection on biotic, abiotic, or prebiotic worlds. *Astrobiology* 2022;22(4):481–493; doi: 10.1089/ast.2021.0079

Blázquez-Blázquez E, Barranco-García R, Cerrada ML, et al. Synchrotron and Raman study of the rotator phases and polymorphism in tricosane paraffin. *Polymers (Basel)* 2020;12(6): 1341; doi: 10.3390/polym12061341

Boynton WV, Bailey SH, Hamara DK, et al. Thermal and evolved gas analyzer: Part of the mars volatile and climate surveyor integrated payload. *J Geophys Res* 2001;106(E8): 17683–17698; doi: 10.1029/1999JE001153

Brinckerhoff WB, Pinnick VT, Van Amerom FH, et al. Mars Organic Molecule Analyzer (MOMA) mass spectrometer for ExoMars 2018 and beyond. IEEE Aerospace Conference 2013; doi: 10.1109/AERO.2013.6496942

Brown ME, Hand KP. Salts and radiation products on the surface of Europa. *Astron. J.* 2013;145(4):110; doi: 10.1088/0004-6256/145/4/110

Broz AP. Organic Matter Preservation in Ancient Soils of Earth and Mars. *Life* 2020;10(7):113; doi: 10.3390/life10070113

Carlson RW, Johnson RE, Anderson MS. Sulfuric acid on Europa and the Radiolytic Sulfur cycle. *Science* 1999; 286(5437):97–99; doi: 10.1126/science.286.5437.97

Carr MH, Belton MJ, Chapman CR, et al. Evidence for a subsurface ocean on Europa. *Nature* 1998;391(6665):363–365; doi: 10.1038/34857

Cheng C, Gross ML. Applications and mechanisms of charge-remote fragmentation. *Mass Spectrom Rev* 2000;19(6):398–420; doi: 10.1002/1098-2787

Chivers CJ, Buffo JJ, Schmidt BE. Stable brine layers beneath Europa's chaos. *Planet Sci J* 2023;4(9):159; doi: 10.3847/PSJ/acea75

Chyba CF. Energy for microbial life on Europa. *Nature* 2000; 403(6768):381–382; doi: 10.1038/35000281

Chyba CF, Phillips CB. Europa as an abode of life. *Orig Life Evol Biosph* 2002;32(1):47–68; doi: 10.1023/A:1013958519734

Cockell CS, Bush T, Bryce C, et al. Habitability: A review. *Astrobiology* 2016;16(1):89–117; doi: 10.1089/ast.2015.1295

Cohen ZR, Todd ZR, Wogan N, et al. Plausible sources of membrane-forming fatty acids on the early earth: A review of the literature and an estimation of amounts. *ACS Earth Space Chem* 2023;7(1):11–27; doi: 10.1021/acsearthspacechem.2c00168

Costello ES, Phillips CB, Lucey PG, et al. Impact gardening on Europa and repercussions for possible biosignatures. *Nat Astron* 2021;5(9):951–956; doi: 10.1038/s41550-021-01393-1

Culka A, Košek F, Oren A, et al. Detection of carotenoids of halophilic prokaryotes in solid inclusions inside laboratory-grown chloride and sulfate crystals using a portable Raman spectrometer: Applications for Mars exploration. *FEMS Microbiol Lett* 2019;366(20):fnz239; doi: 10.1093/femsle/fnz239

Dalton JB, Prieto-Ballesteros O, Kargel JS, et al. Spectral comparison of heavily hydrated salts with disrupted terrains on Europa. *Icarus* 2005;177(2):472–490; doi: 10.1016/j.icarus.2005.02.023

Dartnell LR. Ionizing radiation and life. *Astrobiology* 2011; 11(6):551–582; doi: 10.1089/ast.2010.0528

de Morais Araújo AM, de Oliveira Lima R, Gondim AD, et al. Thermal and catalytic pyrolysis of sunflower oil using AlMCM-41. *Renewable Energy* 2017;101:900–906; doi: 10.1016/j.renene.2016.09.058

Dole M, Milner DC, Williams TF. Irradiation of polyethylene. II. Kinetics of unsaturation effects. *J Am Chem Soc* 1958; 80(7):1580–1588.

Dubravcic MF, Nawar WW. Effect of free fatty acids on the radiolysis of triglycerides. *J Agric Food Chem* 1976;24(5): 1087–1088; doi: 10.1021/jf60207a026

Dubravcic MF, Nawar WW. Radiolysis of lipids: Mode of cleavage in simple triglycerides. *J Am Oil Chem Soc* 1968; 45(10):656–660; doi: 10.1007/BF02541250

Eigenbrode JL. Fossil lipids for life-detection: A case study from the early Earth record. *In: Botta O, Bada JL, Gomez-Elvira J, Javaux E, Selsis F, Summons R editors. Strategies of Life Detection. Space Sci Rev. New York, NY: Springer New York, NY*; 2008; 161–185; doi: 10.1007/978-0-387-77516-6_12

Eigenbrode JL, Summons RE, Steele A, et al. Organic matter preserved in 3-billion-year-old mudstones at Gale crater, Mars. *Science* 2018;360(6393):1096–1101; doi: 10.1126/science.aas9185

Fanale FP, Li YH, De Carlo E, et al. An experimental estimate of Europa's "ocean" composition independent of Galileo orbital remote sensing. *J Geophys Res* 2001;106(E7):14595–14600; doi: 10.1029/2000JE001385

Freitas C, Pereira M, Souza D, et al. Thermal and catalytic pyrolysis of dodecanoic acid on SAPO-5 and Al-MCM-41 catalysts. *Catalysts* 2019;9(5):418; doi: 10.3390/catal9050418

Fréty R, Pacheco JG, Santos MR, et al. Flash pyrolysis of model compounds adsorbed on catalyst surface: A method for screening catalysts for cracking of fatty molecules. *Journal of Analytical and Applied Pyrolysis* 2014;109:56–64; doi: 10.1016/j.jaap.2014.07.013

Georgiou CD, Deamer DW. Lipids as universal biomarkers of extraterrestrial life. *Astrobiology* 2014;14(6):541–549; doi: 10.1089/ast.2013.1134

Gerakines PA, Qasim D, Frail S, et al. Radiolytic destruction of uracil in interstellar and solar system ices. *Astrobiology* 2022; 22(3):233–241; doi: 10.1089/ast.2021.0053

Glavin DP, Freissinet C, Miller KE, et al. Evidence for perchlorates and the origin of chlorinated hydrocarbons detected by SAM at the Rocknest aeolian deposit in Gale Crater. *JGR Planets* 2013;118(10):1955–1973; doi: 10.1002/jgre.20144

Greeley R, Chyba CF, Head JW, et al. Geology of Europa. *In: Bagenal F, Dowling TE, McKinnon WB editors. Jupiter: The planet, satellites and magnetosphere. Cambridge, UK, Cambridge University Press;* 2004; 329–362.

Greeley R, Figueredo PH, Williams DA, et al. Geologic mapping of Europa. *J Geophys Res* 2000;105(E9):22559–22578; doi: 10.1029/1999JE001173

Greenberg R. The icy Jovian satellites after the Galileo mission. *Rep Prog Phys* 2010;73(3):36801; doi: 10.1088/0034-4885/73/3/036801

Greenberg R, Geissler P, Tufts BR, et al. Habitability of Europa's crust: The role of tidal-tectonic processes. *J Geophys Res* 2000; 105(E7):17551–17562; doi: 10.1029/1999JE001147

Gries P, Rathore AS, Lu X, et al. Automated trimethyl sulfonium hydroxide derivatization method for high-throughput fatty acid profiling by gas chromatography–mass spectrometry. *Molecules* 2021;26(20):6246; doi: 10.3390/molecules26206246

Hand KP, Carlson RW. Europa's surface color suggests an ocean rich with sodium chloride. *Geophysical Research Letters* 2015;42(9):3174–3178; doi: 10.1002/2015GL063559

Hand KP, Chyba CF, Priscu JC, et al. Astrobiology and the potential for life on Europa. *Europa* 2009;589–629.

Hau LB, Nawar WW. Radiolysis of lipids in monolayers. I. Saturated fatty acids. *J Americ Oil Chem Soc* 1986;63(5):676–679; doi: 10.1007/BF02638236

Hedges JI, Keil RG. Sedimentary organic matter preservation: An assessment and speculative synthesis. *Marine Chemistry* 1995;49(2–3):81–115; doi: 10.1016/0304-4203(95)00008-F

Hibbitts CA, Stockstill-Cahill K, Wing B, et al. Color centers in salts-evidence for the presence of sulfates on Europa. *Icarus* 2019;326:37–47; doi: 10.1016/j.icarus.2019.02.022

Holdiness MR. Evolved gas analysis by mass spectrometry: A review. *Thermochimica Acta* 1984;75(3):361–399; doi: 10.1016/0040-6031(84)85039-X

Jensen NJ, Gross ML. Mass spectrometry methods for structural determination and analysis of fatty acids. *Mass Spectrometry Reviews* 1987;6(4):497–536; doi: 10.1002/mas.1280060403

Jensen NJ, Tomer KB, Gross ML. Gas-phase ion decomposition occurring remote to a charge site. *J Am Chem Soc* 1985; 107(7):1863–1868.

Johnson RE, Carlson RW, Cooper JF, et al. Radiation effects on the surfaces of the Galilean satellites. *In: Bagenal F, Dowling TE, McKinnon WB editors. Jupiter: The planet, satellites and magnetosphere. Cambridge, UK, Cambridge University Press;* 2004: 485–512.

Jordan SF, Rammu H, Zheludev IN, et al. Promotion of protocell self-assembly from mixed amphiphiles at the origin of life. *Nat Ecol Evol* 2019;3(12):1705–1714; doi: 10.1038/s41559-019-1015-y

Kargel JS, Kaye JZ, Head IJW, et al. Europa's crust and ocean: Origin, composition, and the prospects for life. *Icarus* 2000; 148(1):226–265; doi: 10.1006/icar.2000.6471

Kim KS, Lee JM, Seo HY, et al. Radiolytic products of irradiated authentic fatty acids and triacylglycerides. *Radiation Physics and Chemistry* 2004;71(1–2):47–51; doi: 10.1016/j.radphyschem.2004.04.073

Kivelson MG, Khurana KK, Russell CT, et al. Galileo magnetometer measurements: A stronger case for a subsurface ocean at Europa. *Science* 2000;289(5483):1340–1343; doi: 10.1126/science.289.5483.1340

Kminek G, Bada JL. The effect of ionizing radiation on the preservation of amino acids on Mars. *Earth and Planetary Science Letters* 2006;245(1–2):1–5; doi: 10.1016/j.epsl.2006.03.008

Lai JC, Pearce BK, Pudritz RE, et al. Meteoritic abundances of fatty acids and potential reaction pathways in planetesimals. *Icarus* 2019;319:685–700; doi: 10.1016/j.icarus.2018.09.028

Lewis JMT, Eigenbrode JL, Wong GM, et al. Pyrolysis of oxalate, acetate, and perchlorate mixtures and the implications for organic salts on Mars. *JGR Planets* 2021;126(4):e2020JE006803; doi: 10.1029/2020JE006803

Mahaffy PR, Webster CR, Cabane M, et al. The sample analysis at Mars investigation and instrument suite. *Space Sci Rev* 2012; 170(1–4):401–478; doi: 10.1007/s11214-012-9879-z

Maher KD, Kirkwood KM, Gray MR, et al. Pyrolytic decarboxylation and cracking of stearic acid. *Ind Eng Chem Res* 2008; 47(15):5328–5336; doi: 10.1021/ie0714551

Marion GM, Fritsen CH, Eicken H, et al. The search for life on Europa: Limiting environmental factors, potential habitats, and Earth analogues. *Astrobiology* 2003;3(4):785–811; doi: 10.1089/153110703322736105

Materese CK, Gerakines PA, Hudson RL. The radiation stability of thymine in solid H_2O. *Astrobiology* 2020;20(8):956–963; doi: 10.1089/ast.2019.2199

McKay CP. What is life—and when do we search for it on other worlds. *Astrobiology* 2020;20(2):163–166; doi: 10.1089/ast.2019.2136

Méndez A, Rivera-Valentín EG, Schulze-Makuch D, et al. Habitability models for astrobiology. *Astrobiology* 2021;21(8): 1017–1027; doi: 10.1089/ast.2020.2342

Minoni G, Zerbi G, Rabolt JF. Frequency and intensity patterns of LAM progression in weakly coupled chains: The case of stearic acid and stearyl alcohol. *The Journal of Chemical Physics* 1984;81(11):4782–4789; doi: 10.1063/1.447503

Müller KD, Husmann H, Nalik HP. A new and rapid method for the assay of bacterial fatty acids using high resolution capillary gas chromatography and trimethylsulfonium hydroxide. *Zentralbl Bakteriol* 1990;274(2):174–182; doi: 10.1016/S0934-8840(11)80100-3

Müller K, Schmid EN, Kroppenstedt RM. Improved identification of mycobacteria by using the microbial identification system in combination with additional trimethylsulfonium hydroxide pyrolysis. *J Clin Microbiol* 1998;36(9):2477–2480; doi: 10.1128/jcm.36.9.2477-2480.1998

Nawar WW. Reaction mechanisms in the radiolysis of fats: A review. *J Agric Food Chem* 1978;26(1):21–25.

Nordheim TA, Hand KP, Paranicas C. Preservation of potential biosignatures in the shallow subsurface of Europa. *Nat Astron* 2018;2(8):673–679; doi: 10.1038/s41550-018-0499-8

Nordheim TA, Regoli LH, Harris CD, et al. Magnetospheric ion bombardment of Europa's surface. *Planet Sci J* 2022;3(1):5; doi: 10.3847/PSJ/ac382a

Olszyna-Marzys AE. Radioactivity and foods. *Bulletin of the Pan American Health Organization (PAHO)* 1991;25(1): 1991; doi: 10665.2/27143

Pappalardo RT, Vance S, Bagenal F, et al. Science potential from a Europa lander. *Astrobiology* 2013;13(8):740–773; doi: 10.1089/ast.2013.1003

Paranicas C, Carlson RW, Johnson RE. Electron bombardment of Europa. *Geophys. Res. Lett.* 2001;28(4):673–676; doi: 10.1029/2000GL012320

Paranicas C, Cooper JF, Garrett HB, et al. Europa's radiation environment and its effects on the surface. *Europa* 2009:529–544.

Paranicas C, Mauk BH, Khurana K, et al. Europa's near-surface radiation environment. *Geophys. Res. Lett.* 2007;34(15); doi: 10.1029/2007GL030834

Paranicas C, Ratliff JM, Mauk BH, et al. The ion environment near Europa and its role in surface energetics. *Geophysical Research Letters* 2002;29(5):18; doi: 10.1029/2001GL014127

Parnell J, Cullen D, Sims MR, et al. Searching for life on Mars: Selection of molecular targets for ESA's Aurora ExoMars mission. *Astrobiology* 2007;7(4):578–604; doi: 10.1089/ast.2006.0110

Pavlov AA, McLain HL, Glavin DP, et al. Rapid radiolytic degradation of amino acids in the Martian shallow subsurface: Implications for the search for extinct life. *Astrobiology* 2022;22(9):1099–1115; doi: 10.1089/ast.2021.0166

Pavlov AA, Vasilyev G, Ostryakov VM, et al. Degradation of the organic molecules in the shallow subsurface of Mars due to irradiation by cosmic rays. *Geophys. Res. Lett.* 2012; 39(13); doi: 10.1029/2012GL052166

Pavlov AA, McLain H, Glavin DP, et al. Radiolytic effects on biological and abiotic amino acids in shallow subsurface ices on Europa and Enceladus. *Astrobiology* 2024;24(7):698–709; doi: 10.1089/ast.2023.0120

Roach LH, Mustard JF, Murchie SL, et al. Testing evidence of recent hydration state change in sulfates on Mars. *J Geophys Res* 2009;114(E2); doi: 10.1029/2008JE003245

Scheeder G, Weniger P, Blumenberg M. Geochemical implications from direct rock-eval pyrolysis of petroleum. *Organic Geochemistry* 2020;146:104051; doi: j.orggeochem.2020.104051

Scheidema MN, Taskinen P. Decomposition thermodynamics of magnesium sulfate. *Ind Eng Chem Res* 2011;50(16): 9550–9556; doi: 10.1021/ie102554f

Schmidt BE, Blankenship DD, Patterson GW, et al. Active formation of 'chaos terrain' over shallow subsurface water on Europa. *Nature* 2011;479(7374):502–505; doi: 10.1038/nature10608

Schubert G, Sohl F, Hussmann H. Interior of Europa. *Europa* 2009;35:3–67.

Sephton MA, Botta O. Extraterrestrial organic matter and the detection of life. *In: Botta O, Bada JL, Gomez-Elvira J, Javaux E, Selsis F, Summons R editors. Strategies of Life Detection. Space Sci Rev. New York, NY: Springer New York, NY;* 2008;135(1–4):25–35; doi: 10.1007/s11214-007-9171-9

Sephton MA, Botta O. Recognizing life in the solar system: Guidance from meteoritic organic matter. *International Journal of Astrobiology* 2005;4(3–4):269–276; doi: 10.1017/S1473550405002806

Shadkami F, Estevez S, Helleur R. Analysis of catechins and condensed tannins by thermally assisted hydrolysis/methylation-GC/MS and by a novel two step methylation. *Journal of Analytical and Applied Pyrolysis* 2009;85(1–2):54–65; doi: 10.1016/j.jaap.2008.09.001

Sharma SK, Porter JN, Misra AK, et al. Standoff Raman spectroscopy for future Europa lander missions. *J Raman Spectroscopy* 2020;51(9):1782–1793; doi: 10.1002/jrs.5814

Sharma S, Roppel RD, Murphy AE, et al. Diverse organic-mineral associations in Jezero crater, Mars. *Nature* 2023; 619(7971):724–732; doi: 10.1038/s41586-023-06143-z

Snåre M, Kubičková I, Mäki-Arvela P, et al. Heterogeneous catalytic deoxygenation of stearic acid for production of biodiesel. *Ind Eng Chem Res* 2006;45(16):5708–5715; doi: 10.1021/ie060334i

Sparks WB, Schmidt BE, McGrath MA, et al. Active cryovolcanism on Europa? *ApJL* 2017;839(2):L18; doi: 10.3847/2041-8213/aa67f8

Summons RE, Albrecht P, McDonald G, et al. Molecular biosignatures. *In: Botta O, Bada JL, Gomez-Elvira J, Javaux E, Selsis F, Summons R editors. Strategies of Life Detection. Space Sci Rev. New York, NY: Springer New York, NY;* 2008:133–159; doi: 10.1007/978-0-387-77516-6_11

Trainer MG, Brinckerhoff WB, Grubisic A, et al. Development of the dragonfly mass spectrometer (DraMS) for Titan. In Lunar and Planetary Science Conference 2021.

Vajdi M, Nawar WW, Merritt C. Comparison of radiolytic compounds from saturated and unsaturated triglycerides and fatty acids. *J Am Oil Chem Soc* 1978;55(22):849–850; doi: 10.1007/BF02671403

Veneranda M, Lopez-Reyes G, Manrique JA, et al. ExoMars Raman laser spectrometer: A tool for the potential recognition of wet-target craters on mars. *Astrobiology* 2020;20(3): 349–363; doi: 10.1089/ast.2019.2095

Vitkova A, Walker SJ, Sykulska-Lawrence H. The impact of extreme low temperatures on Raman spectra of amino acids relevant for the search for life on Europa. *Astrobiology* 2022; 22(11):1271–1292; doi: 10.1089/ast.2021.0136

Wang A, Freeman JJ, Jolliff BL, et al. Sulfates on Mars: A systematic Raman spectroscopic study of hydration states of magnesium sulfates. *Geochimica et Cosmochimica Acta* 2006;70(24):6118–6135; doi: 10.1016/j.gca.2006.05.022

Warren CH, Hooper DL. Chain length determination of fatty acids by Raman spectroscopy. *Can J Chem* 1973;51(23): 3901–3904; doi: 10.1139/v73-581

Woo L, Sandford CL. Comparison of electron beam irradiation with gamma processing for medical packaging materials. *Radiation Physics and Chemistry* 2002;63(3–6):845–850; doi: 10.1016/S0969-806X(01)00664-8

Wu GS, Howton DR. γ-radiolysis of stearic acid: Studies of nongaseous products. *Radiat Res* 1975;61(3):374–392; doi: 10.2307/3574113

Zolotov MY, Shock EL. Composition and stability of salts on the surface of Europa and their oceanic origin. *J Geophys Res* 2001;106(E12):32815–32827; doi: 10.1029/2000JE001413

Address correspondence to:
James M.T. Lewis
Department of Physics and Astronomy
Howard University
Washington
District of Columbia
USA

E-mail: James.m.lewis@nasa.gov

Submitted April 22, 2024
Accepted October 31, 2024
Associate Editor: Lewis Dartnell

Abbreviations Used

CRF = Charge remote fragmentation
DCM = Dichloromethane
EGA-MS = Evolved gas analysis mass spectrometry

Abbreviations Used (Cont.)

EI = Electron ionization
FAME = Fatty acid methyl ester
GC = Gas chromatograph/gas chromatography
GCMS = Gas chromatograph mass spectrometer/ gas chromatography mass spectrometry
LAM = Longitudinal acoustic mode
LDI-MS = Laser desorption and ionization mass spectrometry
MS = Mass spectrometer/mass spectrometry
MSD = Mass Selective Detector
m/z = Mass to charge ratio
N.D. = No detection
NIST = National Institute of Standards & Technology
RPM = Revolutions per minute
RSEC = Radiation Science & Engineering Center
THM = Thermally assisted hydrolysis and methylation
TMSH = Trimethylsulfonium hydroxide